DOT/FAA/AEE/2012-03
DOT-VNTSC-FAA-12-05.I

ASSESSMENT OF THE HYBRID PROPAGATION MODEL

VOLUME 1: ANALYSIS OF NOISE PROPAGATION EFFECTS

Joyce E. Rosenbaum
Eric R. Boeker
Alexandre Buer
Paul J. Gerbi
Cynthia S. Y. Lee
Christopher J. Roof
Gregg G. Fleming

U.S. Department of Transportation
Research and Innovative Technology Administration
John A. Volpe National Transportation Systems Center
Environmental Measurement and Modeling Division, RVT-41
Kendall Square
Cambridge, MA 02142

August 2012
Final Report

U.S. Department of Transportation
Federal Aviation Administration

REPORT DOCUMENTATION PAGE

Form Approved
OMB No. 0704-0188

1. AGENCY USE ONLY (Leave blank)	2. REPORT DATE	3. REPORT TYPE AND DATES COVERED
	August 2012	Final Report

4. TITLE AND SUBTITLE
Assessment of the Hybrid Propagation Model, Volume 1: Analysis of Noise Propagation Effects

5. FUNDING NUMBERS
FP01 (JD7RC),
FA4SC3 (KJ200)

6. AUTHOR(S)
Joyce Rosenbaum, Eric Boeker, Alexandre Buer, Paul Gerbi, Cynthia Lee, Christopher Roof, Gregg Fleming

7. PERFORMING ORGANIZATION NAME(S) AND ADDRESS(ES)
U.S. Department of Transportation
Research and Innovative Technology Administration
John A. Volpe National Transportation Systems Center
Environmental Measurement and Modeling Division, RVT-41
Cambridge, MA 02142-1093

8. PERFORMING ORGANIZATION REPORT NUMBER
DOT-VNTSC-FAA-12-05.I

9. SPONSORING/MONITORING AGENCY NAME(S) AND ADDRESS(ES)
U.S. Department of Transportation
Federal Aviation Administration
Office of Environment and Energy, AEE-100
Washington, DC 20591

10. SPONSORING/MONITORING AGENCY REPORT NUMBER
DOT/FAA/AEE/2012-03

11. SUPPLEMENTARY NOTES
FAA Program Managers: Barry Brayer and Keith Lusk (AWP, Western-Pacific Regional Office, Special Programs Staff); Rebecca Cointin and Bill He (AEE, Office of Environment and Energy, Noise Division)

12a. DISTRIBUTION/AVAILABILITY STATEMENT

12b. DISTRIBUTION CODE

13. ABSTRACT (Maximum 200 words)

This is the first of two volumes of a report on the Hybrid Propagation Model (HPM), an advanced prediction model for aviation noise propagation. This volume presents the noise level predictions for eleven different sets of propagation conditions, run by the HPM. The conditions include effects of uneven terrain, refractive atmosphere, and ground type transitions. The results are analyzed in detail and comparisons are made across four different source altitudes and between the different component models of the HPM. In addition, a scheme of “intelligent switching” between the HPM’s component models is posed as an approach to address the long runtimes of the HPM. The feasibility of this strategy is discussed and some points of caution regarding its implementation are identified. HPM results are compared to the Integrated Noise Model (INM) under uneven terrain conditions in Volume 2 of this report. The goal of this research is to enhance the modeling capabilities of the Aviation Environmental Design Tool (AEDT) and INM, particularly in complicated environments such as National Parks.

14. SUBJECT TERMS	15. NUMBER OF PAGES
Aircraft Noise, Noise Prediction, Noise Model Comparison, Hybrid Propagation Model, Integrated Noise Model, Parabolic Equation, Fast Field Program, Ray Model	44
	16. PRICE CODE

17. SECURITY CLASSIFICATION OF REPORT	18. SECURITY CLASSIFICATION OF THIS PAGE	19. SECURITY CLASSIFICATION OF ABSTRACT	20. LIMITATION OF ABSTRACT
Unclassified	Unclassified	Unclassified	

METRIC/ENGLISH CONVERSION FACTORS

ENGLISH TO METRIC

LENGTH (APPROXIMATE)

1 inch (in)	=	2.5 centimeters (cm)
1 foot (ft)	=	30 centimeters (cm)
1 yard (yd)	=	0.9 meter (m)
1 mile (mi)	=	1.6 kilometers (km)

AREA (APPROXIMATE)

1 square inch (sq in, in^2)	=	6.5 square centimeters (cm^2)
1 square foot (sq ft, ft^2)	=	0.09 square meter (m^2)
1 square yard (sq yd, yd^2)	=	0.8 square meter (m^2)
1 square mile (sq mi, mi^2)	=	2.6 square kilometers (km^2)
1 acre = 0.4 hectare (he)	=	4,000 square meters (m^2)

MASS – WEIGHT (APPROXIMATE)

1 ounce (oz)	=	28 grams (gm)
1 pound (lb)	=	0.45 kilogram (kg)
1 short ton = 2,000 pounds (lb)	=	0.9 tonne (t)

VOLUME (APPROXIMATE)

1 teaspoon (tsp)	=	5 milliliters (ml)
1 tablespoon (tbsp)	=	15 milliliters (ml)
1 fluid ounce (fl oz)	=	30 milliliters (ml)
1 cup ©	=	0.24 liter (l)
1 pint (pt)	=	0.47 liter (l)
1 quart (qt)	=	0.96 liter (l)
1 gallon (gal)	=	3.8 liters (l)
1 cubic foot (cu ft, ft^3)	=	0.03 cubic meter (m^3)
1 cubic yard (cu yd, yd^3)	=	0.76 cubic meter (m^3)

TEMPERATURE (EXACT)

[(x-32)(5/9)] °F	=	y °C

METRIC TO ENGLISH

LENGTH (APPROXIMATE)

1 millimeter (mm)	=	0.04 inch (in)
1 centimeter (cm)	=	0.4 inch (in)
1 meter (m)	=	3.3 feet (ft)
1 meter (m)	=	1.1 yards (yd)
1 kilometer (km)	=	0.6 mile (mi)

AREA (APPROXIMATE)

1 square centimeter (cm^2)	=	0.16 square inch (sq in, in^2)
1 square meter (m^2)	=	1.2 square yards (sq yd, yd^2)
1 square kilometer (km^2)	=	0.4 square mile (sq mi, mi^2)
10,000 square meters (m^2)	=	1 hectare (ha) = 2.5 acres

MASS – WEIGHT (APPROXIMATE)

1 gram (gm)	=	0.036 ounce (oz)
1 kilogram (kg)	=	2.2 pounds (lb)
1 tonne (t)	=	1,000 kilograms (kg)
	=	1.1 short tons

VOLUME (APPROXIMATE)

1 milliliter (ml)	=	0.03 fluid ounce (fl oz)
1 liter (l)	=	2.1 pints (pt)
1 liter (l)	=	1.06 quarts (qt)
1 liter (l)	=	0.26 gallon (gal)
1 cubic meter (m^3)	=	36 cubic feet (cu ft, ft^3)
1 cubic meter (m^3)	=	1.3 cubic yards (cu yd, yd^3)

TEMPERATURE (EXACT)

[(9/5) y + 32] °C	=	x °F

QUICK INCH - CENTIMETER LENGTH CONVERSION

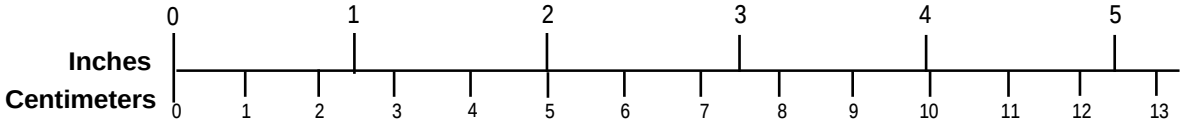

QUICK FAHRENHEIT - CELSIUS TEMPERATURE CONVERSIO

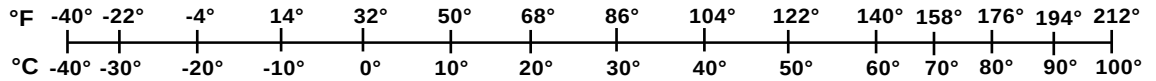

For more exact and or other conversion factors, see NIST Miscellaneous Publication 286, Units of Weights and Measures. SD Catalog No. C13 10286

Table of Contents

1. INTRODUCTION

The hybrid propagation model (HPM)[1,2] is a numerical model designed to predict aviation noise levels under complicated propagation conditions. The goal of this research is to enhance the modeling capabilities of the FAA's Aviation Environmental Design Tool (AEDT) and Integrated Noise Model (INM) in complex environments, such as National Parks. The model was originally developed in a research effort at the Pennsylvania State University in cooperation with the Volpe National Transportation Systems Center and the Federal Aviation Administration (FAA). HPM is a composite of three propagation methods: a parabolic equation (PE) model; a fast field program (FFP); and a straight ray-trace model. This report presents a study of various propagation conditions run by HPM and its component models. Comparisons were also made between the full HPM, a pure FFP, and a pure ray model. In the "Assessment of the Hybrid Propagation Model, Volume 2: Comparison with the Integrated Noise Model" report[3], comparisons between the HPM and the AEDT/INM are presented. Analyses of the more complicated propagation conditions provide a foundation upon which to develop criteria for reducing computation time of noise level predictions - that is, identifying conditions that do not demand the advanced capabilities of the full HPM, but rather can afford to be run by a simpler, faster method. A detailed comparison of these cases reveals how to utilize the HPM and its component models most efficiently.

The three component models of the HPM were chosen for their complementary strengths. The PE allows the HPM to incorporate range-dependent effects at small elevation angles from the source, such as terrain features, transitions between different types of ground, and changing meteorology. The FFP ensures that the model is accurate at low frequencies to moderate elevation angles, for cases without extreme range-dependent changes near the source. The straight-ray model fills in levels at the higher elevation angles, where the accuracy of the other two models is degraded. The resulting HPM model can return noise levels at all points in the vertical, line-of-sight slice between the source and a distant receiver.

2. OVERVIEW OF THE COMPONENT MODELS

The PE model used in the HPM is a two-dimensional generalized terrain, finite difference formulation[4,5,6]. It is derived from the one-way Helmholtz equation[6] with use of an assumption that limits the validity of the model to elevation angles up to approximately ±35 degrees from the horizontal of the source. The PE propagates sound in the two-dimensional vertical plane by extrapolating results at one range step from results at previous range steps, and it incorporates range-dependent effects at small elevation angles from the source, such as terrain features, transitions between different types of ground, and changing meteorology. However, because it is derived from the one-way Helmholtz equation, it can only account for sound moving in the forward direction from the source to the receiver and does not include backscatter.

Because of the elevation angle limitation of the PE, the HPM utilizes the FFP in conjunction with the PE. The FFP[6,7,8] is derived from the Helmholtz equation by applying a transformation from the horizontal spatial domain into the horizontal wave number domain. It propagates sound in the two-dimensional vertical plane between stratified layers of the atmosphere. The FFP, accurate both at low frequencies and at moderate elevation angles, supplements the PE. It is, however, limited to inclusion of non-range-dependent propagation effects, and errors are introduced at higher elevation angles from the effects of a window applied in the horizontal wave number domain. The valid angle range depends on the steepness of the window roll-off. The window used in the calculations of this report introduces inaccuracies at angles above 72 degrees. However, to be conservative, a smaller angle range below 48 degrees was used.

Finally, a straight-ray model is used to fill in the regions of the steepest emission angles from the source. This model is a superposition of the direct and reflected sound at the receiver point, assuming the sound follows a straight path. While it can include the effects of a uniform, finite-impedance ground, it incorporates neither range-dependent effects, nor refractive atmospheres. More advanced ray models, however, are able to incorporate these propagation effects. The straight-ray model was used in this research for its quick development time and because it is needed only for the smallest ranges, where range-dependent effects will have a minimal effect.

The construction of the hybrid model is achieved by joining the ray, FFP, and PE components in the appropriate regions in the two-dimensional vertical plane, as shown in Figure 1. PE results are used in elevation angles of 35 degrees and below, FFP results are used between 35 and 48 degrees, and ray results are used above 48 degrees. The performance of both individual PE and FFP models was verified against both analytical solutions and published results[6,9]. The ray model was verified against the PE and FFP models. Their agreement can be seen in results presented for simple propagation cases, in Sections 4.1 and 4.2. Merging them into a hybrid model is validated in this report through running test cases that explore results of different source heights and frequencies, as well as propagation conditions.

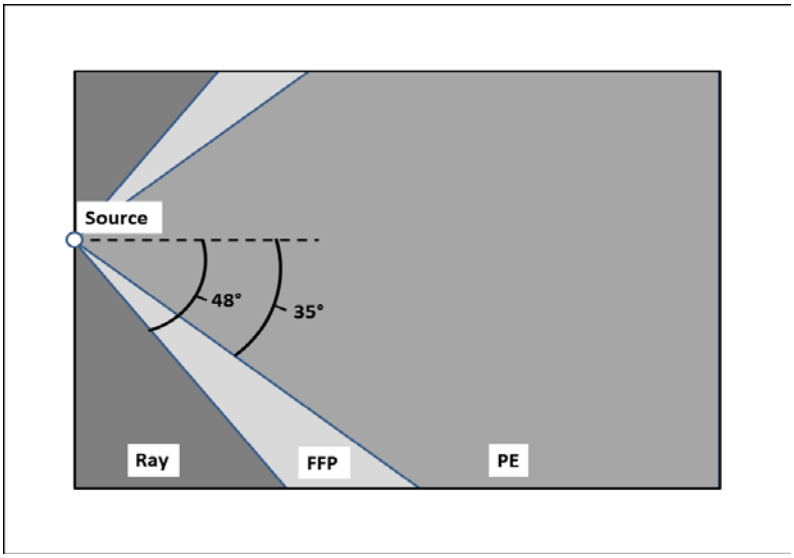

Figure 1. Combination of component models in HPM in the vertical plane

3. HPM PROGRAMMING IMPLEMENTATION

Different programming language options have been explored for use in the ultimate implementation of HPM. Originally developed in MATLAB®, the HPM has also been translated into F# with the goal of offering a version capable of seamless integration into the .NET framework and AEDT. However, operations on large matrices are a substantial contributor to the computations required by the HPM. The F# language does not currently offer an efficient implementation of large matrix operations and, therefore, the F# code version was tabled and a compiled version of MATLAB code with a C# "wrapper" is currently used. The compiled MATLAB code takes advantage of the MATLAB matrix operation implementation capabilities, while retaining the capacity to run HPM within the .NET framework, and without the need of a MATLAB license.

An AEDT research testing interface was developed to accept necessary HPM input parameters that define meteorology and ground-type conditions. Information about the source-receiver geometry is extracted from a "flight.pth" file input and terrain profile data is extracted from a grid float file, to allow for easier integration with AEDT's Aircraft Acoustics Module (AAM). All necessary inputs are written to an XML file that is read by the HPM. The current HPM implementation in the testing interface has been verified with previous versions of the HPM to ensure no errors were introduced in the code transformation.

4. HPM TEST CASES

Eleven different test cases are considered in this report. They were designed to be simple enough for pointed, systematic study, and yet representative of certain aspects of real world applications. A base case is presented first (Case 1) as a control condition for the remaining cases. The base case includes a flat, soft ground and a homogeneous atmosphere. The next 9 cases each isolate a single propagation mechanism and consider its effect on the base case results. Case 2 uses a hard, flat ground and a homogeneous atmosphere; Cases 3 and 4 use a soft, flat ground with an upward and downward refracting atmosphere, respectively; Cases 5, 6, and 7 use a soft ground with a hill, upward sloping, or downward sloping ground, respectively, and a homogeneous atmosphere; Cases 8 and 9 use transitions from hard to soft ground, or soft to hard ground, respectively, with flat terrain and a homogeneous atmosphere; Case 10 uses two ground-type transitions, first from hard to soft ground and then back to hard ground, with flat terrain and a homogeneous atmosphere. The mechanisms can be broken into three categories of effects: ground type, terrain, and meteorology. The final case (Case 11) combines all three categories of effects, using a ground that transitions from hard to soft to hard, a hill terrain feature, and a downward refracting atmosphere. The combination of effects offers a realistic propagation case and provides insight into how the effects interact.

Diagrams of the geometries of each case are shown in Figure 2. Green, solid lines indicate soft ground and brown, dashed lines indicate hard ground. Each condition consists of a point source at a given altitude. Results are presented as a function of horizontal range from the source for a receiver at a given height above the ground. Four source heights are considered for each case. The common parameters are listed below.

- Source heights (measured from the ground surface directly below): 10, 40, 100, 400 m
- Source noise and performance data[*]: 747-400 overflight, 7444 lbs thrust, the A-weighted maximum sound level (LAMAX) metric
- Receiver height (above the ground surface): 1.219 m
- Soft Ground, Hard Ground: Effective flow resistivities of 150 and 20,000 cgs Rayls, respectively
- Temperature: 14.9 °C

The broadband results are presented as A-weighted maximum sound levels for the given aircraft source. These are generated by calculating the attenuations of propagation with respect to the level 1 m from the source using the HPM or component models, separately for each one-third octave band. The attenuations are applied to the source data, which also conform to the 1 m distance from the source, for each one-third octave band. Finally, all of the propagated band levels are logarithmically summed to obtain the broadband results for the aircraft source.

[*] HPM source noise data are developed from INM/AEDT source data [Noise-Power-Distance (NPDs) curves and spectral class]. The appropriate spectral class is calibrated to the aircraft-specific NPD at 1000 ft (305 m). Then, the calibrated spectrum is propagated back to a distance of 1 m from the source using the method described in SAE-AIR-1845 and FAR 36, assuming the ICAO standard atmosphere.

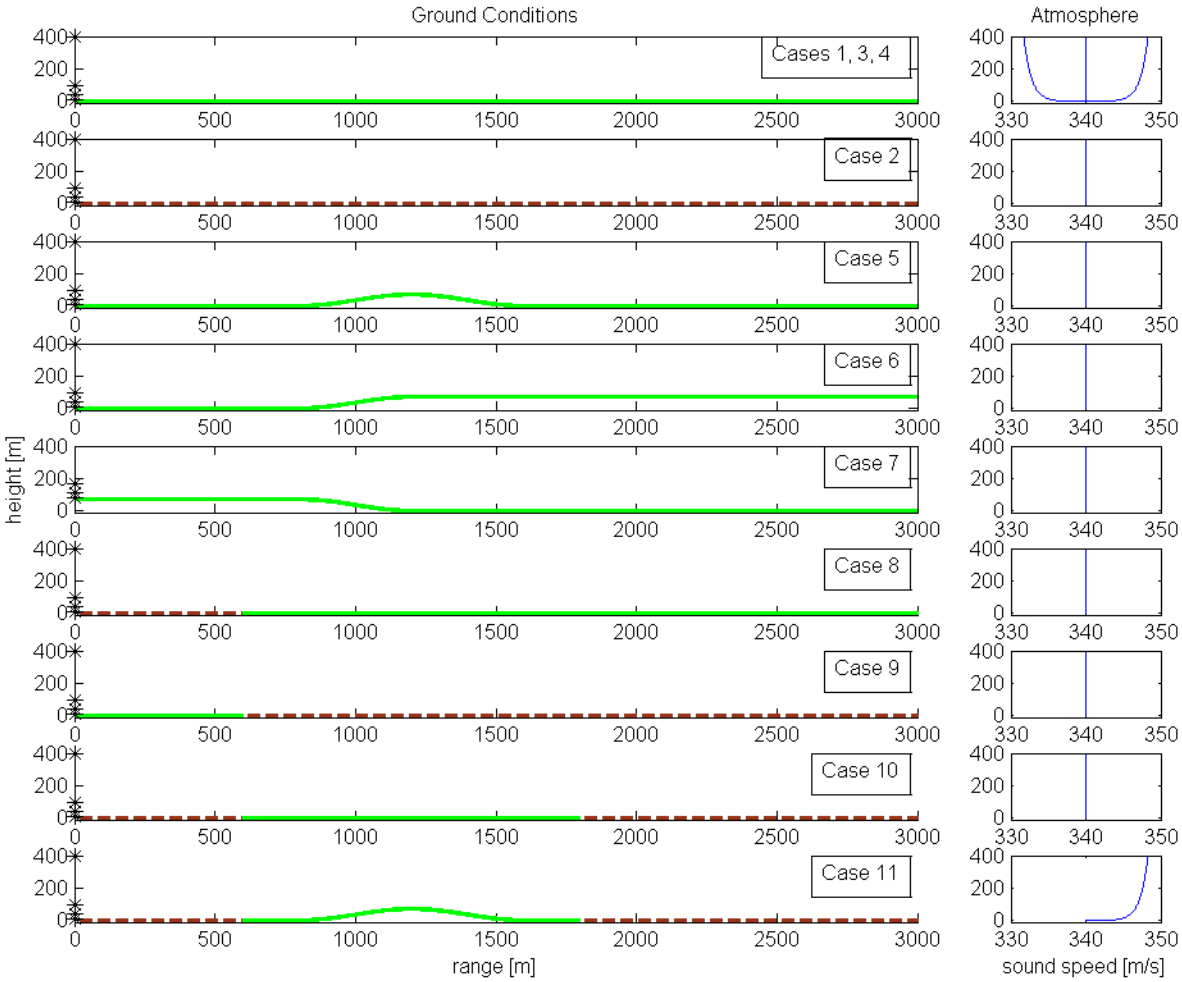

Figure 2. Diagrams of the ground and atmospheric conditions of the eleven test cases (green, solid lines indicate soft ground and brown, dashed lines indicate hard ground)

While the HPM is meant to be a standalone model in its current form, unfeasibly long runtimes are a concern. An initial investigation of conditions under which a faster, simpler model is sufficiently accurate to capture all significant effects on propagation is discussed in Section 6. Such a study is valuable in developing a protocol of "intelligent switching," by which the propagation model used is selected according to the specific needs of the current propagation conditions. For example, in the simplest conditions of Base Case 1, a flat, soft ground and homogeneous atmosphere, the straight-ray model may be sufficiently accurate. Conversely, the hill condition of Case 5, with a low altitude source, would benefit from running the full HPM. Therefore, in addition to generating results for the full hybrid implementation, separate runs were performed using the pure FFP and the pure ray models for comparison, where applicable.

Computational resources used in the test case runs include a Dell Precision laptop with an Intel Core i7-2720QM processor and 8 GB RAM, 2 nodes of an AEDT server each with 8 cores, an Intel Xeon E5520 processor, and 24 GB RAM, referred to as Server 1, and a server with 8 cores, an Intel Xeon E5405 processor, and 8 GB RAM (Server 2). Runtimes for the full HPM implementations ranged from between about 2.5 days for Base Case 1, run on the laptop, to over

5 days for Cases 6 and 11, run on the nodes of Server 1. Runtimes for the FFP implementation were between a little over 1 day for Case 3, run on a node of Server 1, and about 2.5 days for Case 2, run on Server 2. All ray model runs took less than a minute. These runtimes reflect clock times, during which all four sources are run in parallel and, within each source, each individual frequency of the spectrum is run serially.

A comparison between HPM and INM is presented in Volume 2 of this report[3], for four of eleven cases for which INM can incorporate the considered propagation mechanisms: the base, hill, upward sloping terrain, and downward sloping terrain cases (Cases 1, 5, 6, and 7, respectively).

4.1 Base Case 1: Soft, Flat Ground, Homogeneous Atmosphere

Base Case 1 uses the simplest set of propagation conditions: a soft, flat ground with a homogeneous atmosphere. It serves both as a starting point of comparison between the component models, and between the four different source height conditions, and also as the baseline for evaluating the added effects of more complicated mechanisms in propagation.

Figure 3 shows results for Base Case 1, separately, for the 4 different source heights. Each subfigure plots HPM, FFP, and ray model results. HPM results are composed of ray results at the smallest ranges, then FFP results for the moderately small ranges, and PE results for the remainder of the range. The FFP and ray results are calculated exclusively with the FFP and ray models, respectively.

For each source, levels decrease with distance, resulting from geometrical spreading, atmospheric absorption and the effect of the soft ground. Some fluctuations in level can be seen for all four sources, especially toward the lower ranges, as a result of the interference patterns of the discrete frequencies. The combination of the twenty-four one-third octave band results, however, smoothes the severe interference pattern peaks and dips of the individual frequency bands.

Aside from results at the smallest ranges, where the FFP accuracy is degraded, the results of the three models agree well and the plotted HPM, FFP, and RAY result lines are nearly indistinguishable. At the smaller ranges, before the transition to use of the PE in the HPM model, the comparison is only between FFP and ray model results. At the larger ranges, the comparison is between PE, FFP, and ray model results. The ranges of model transitions within the HPM can be seen in the results figures, denoted by vertical, black arrows. Because the model transition ranges for the lowest three sources are small compared to the overall propagation ranges, the arrows overlap to varying degrees.

For this simple set of propagation conditions—soft, flat ground and a homogeneous atmosphere—the agreement between the three models indicates that, so long as the model is considered to be accurate in the propagation region of interest, the choice of model is insignificant.

Figure 4 shows a comparison between the results of HPM for the four different source heights. Note that because of the good agreement between the three models, only one model is needed for the comparison of the four source heights - here the HPM is used. As expected, levels at smaller ranges are larger for lower altitude sources, the result of smaller source-receiver distances. However, the effect of the soft ground is seen in the reduced levels for lower altitude source heights, at longer ranges. The shallower angles of reflection of sound off the ground for lower altitude sources lead to lower overall levels. The levels at 3 km are 28.5 dB, 40.1 dB, 46.7 dB, and 50.4 dB for the 10 m, 40 m, 100 m, and 400 m sources, respectively. The spread in level among the four source heights at a range of 3 km is 21.9 dB.

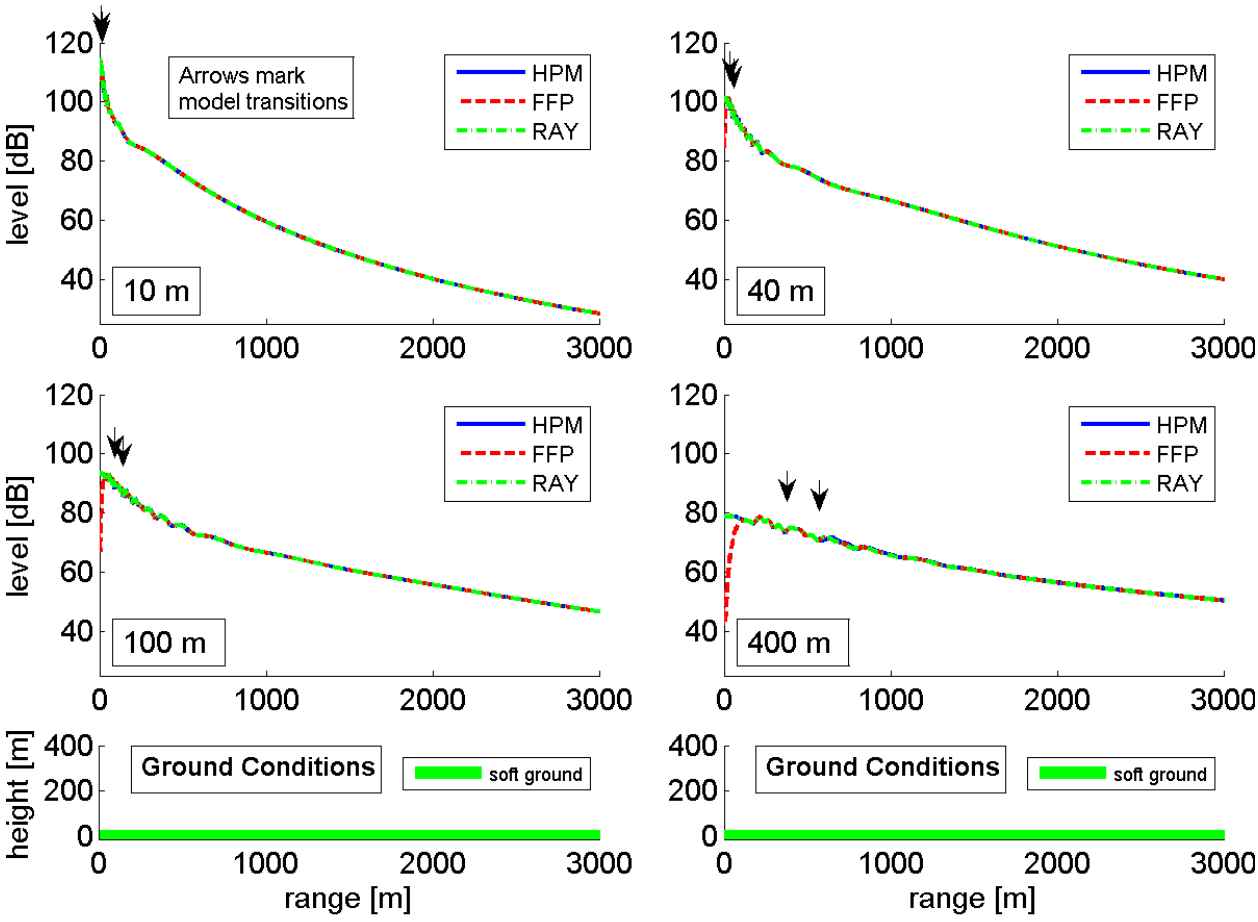

Figure 3. Base Case 1—Soft, flat ground and homogeneous atmosphere. HPM, FFP, and RAY results compared for each source height—10 m, 40 m, 100 m, and 400 m. Results of the three models overlap over most of the range. A diagram of the propagation conditions is included beneath the results figures.

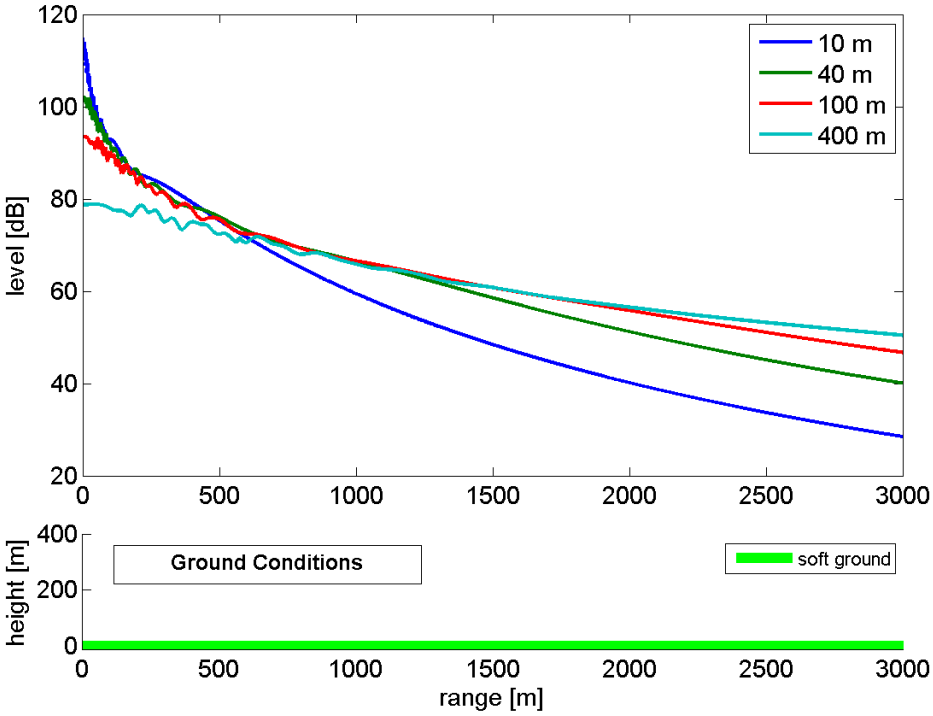

Figure 4. Base Case 1—Soft, flat ground and homogeneous atmosphere. HPM results for each source height—10 m, 40 m, 100 m, and 400 m—plotted together. A diagram of the propagation conditions is included beneath the results figure.

4.2 Case 2: Hard, Flat Ground, Homogeneous Atmosphere

Case 2 is similar to Base Case 1, but uses hard ground in place of soft. Results of the three models (HPM, FFP, and ray), are seen in Figure 5 for each source height. Again, the models agree well in the region where all models are valid.

The HPM results for Base Case 1 are also included in the comparison for each source height. A comparison between the hard and soft ground results shows agreement at ranges below approximately 400 m. The results of Cases 1 and 2 begin to diverge at longer ranges, with larger levels recorded for the hard ground case, as expected. The differences increase with range and decrease with source height. At the horizontal propagation range of 3 km, the differences between Case 2 and Base Case 1 results for the 10, 40, 100, and 400 m source heights are 26.1, 14.7, 8.1, and 1.8 dB, respectively.

Again, the comparison of the three models—HPM, FFP, and ray—under these propagation conditions, indicates that the choice of model is unimportant, as long as the model is considered to be accurate in the propagation region of interest.

Figure 6 shows a comparison of HPM results for the four source heights. Here, again, the lower altitude sources show larger levels at the smallest ranges because the receivers are closer to the

sources. However, the lower levels for low altitude sources at larger ranges are no longer seen in the hard ground case, as they had been in Base Case 1. In fact, for hard ground, the highest altitude source has the lowest level, as predicted by spherical spreading and atmospheric absorption attenuation effects. Overall levels at 3 km for the 10, 40, 100, and 400 m sources are 54.6, 54.7, 54.9, and 52.2 dB, respectively. The spread in level among the four source heights at a range of 3 km is only 2.4 dB.

The comparison between Cases 1 and 2 demonstrates that ground type has a fairly minimal effect at small ranges (below approximately 400 m for the geometries explored in this report). However, it has a significant impact for lower altitude sources and longer propagation ranges.

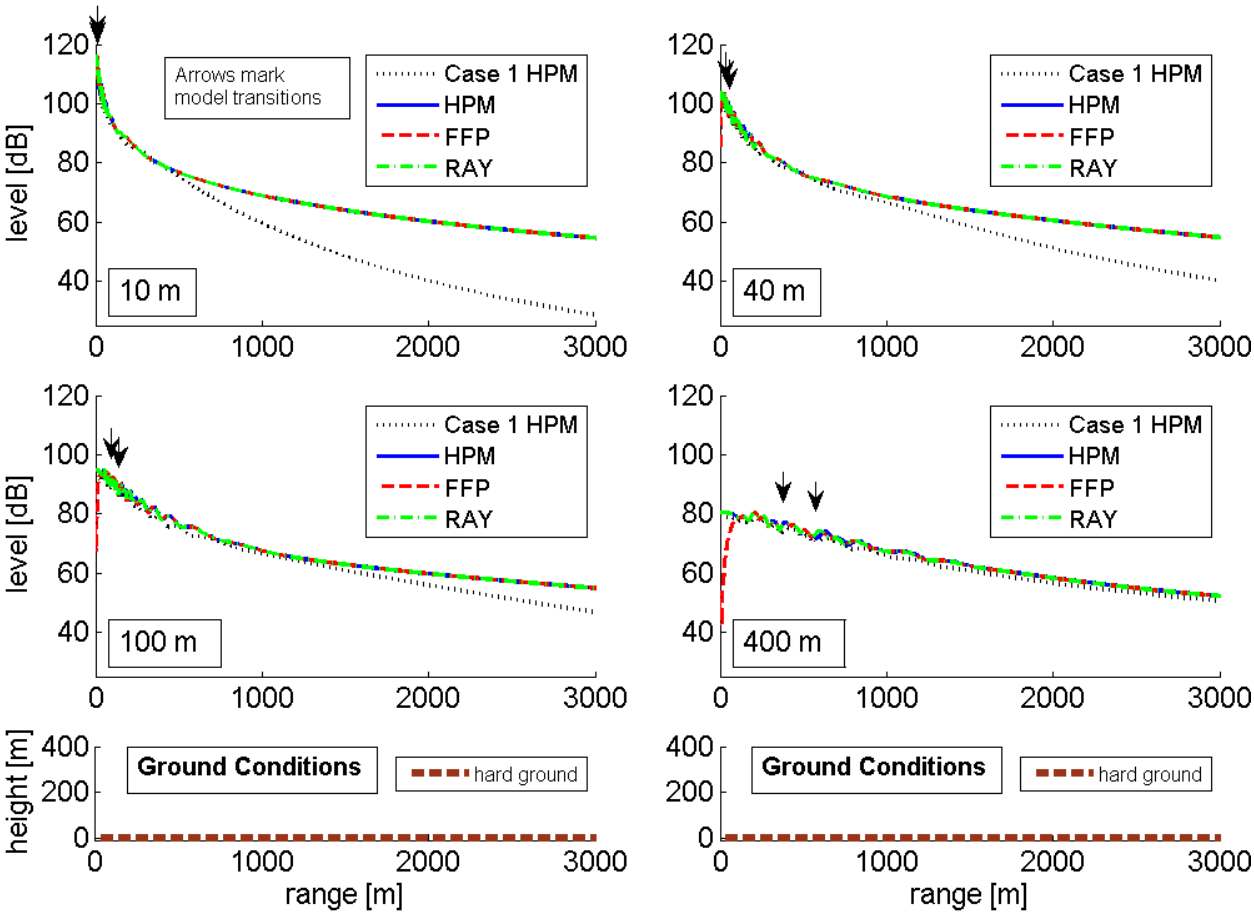

Figure 5. Case 2—Hard, flat ground and homogeneous atmosphere. HPM, FFP, and RAY results compared for each source height—10 m, 40 m, 100 m, and 400 m. Results of the three models overlap over most of the range. Base Case 1 HPM results are included for comparison. A diagram of the propagation conditions is included beneath the results figures.

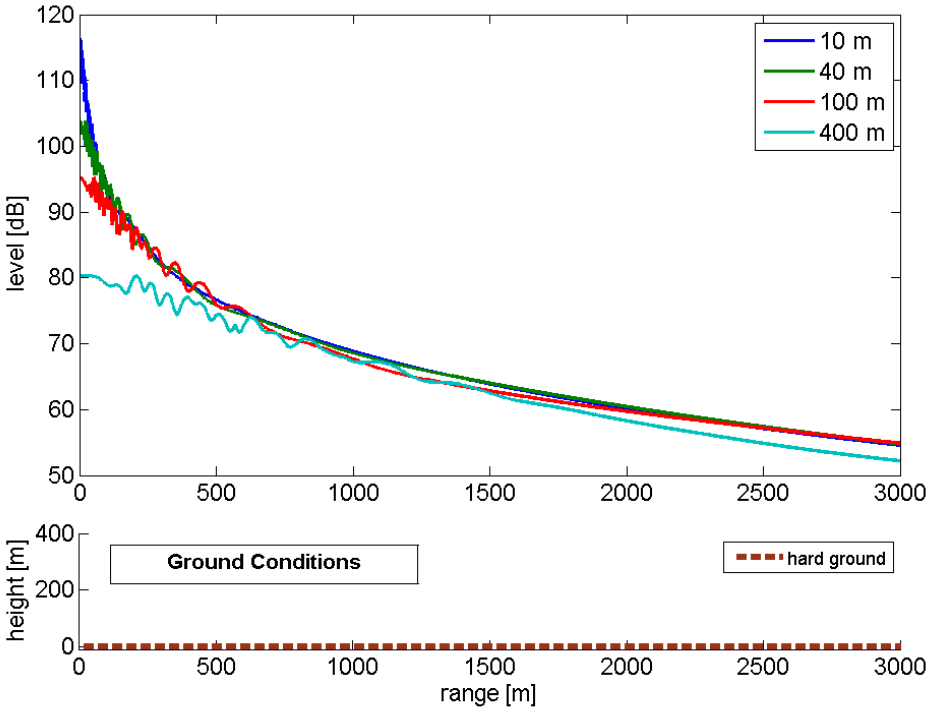

Figure 6. Case 2—Hard, flat ground and homogeneous atmosphere. HPM results for each source height—10 m, 40 m, 100 m, and 400 m—plotted together. A diagram of the propagation conditions is included beneath the results figure.

4.3 Case 3: Soft, Flat Ground, Upward Refracting Atmosphere

Case 3 differs from Base Case 1 in its applied atmospheric conditions. An upward refracting atmosphere, used in Case 3, can result either from wind—in upwind conditions—or from a negative thermal gradient—in daytime conditions when air temperature decreases with height. A logarithmic refracting atmosphere is used in this report, defined by the equation

$$C(z) = c_0 + [b \times ln(\frac{z}{z_0} + 1)] \quad (1)$$

where

- c_o sound speed at the ground,
- b logarithmic sound speed profile parameter,
- z_o aerodynamic roughness length of the ground surface, and
- z height above the ground.

For the two refractive atmosphere conditions explored, values of c_o = 340.2 m/s and z_o = 0.1 m are applied. In Case 3, upward refracting atmosphere conditions, a logarithmic sound speed profile parameter of b = -1 m/s is used.

Figure 7 shows the comparison between HPM and FFP results for each source height. The ray model is not included because it was not developed to incorporate a refractive atmosphere. However, the capability could be added in future work. Again, the HPM Base Case 1 results are included for comparison. While the HPM data were chosen to represent the base case for comparison, they could be thought of as a stand-in for any of the three models, which all yield

very similar results in Base Case 1. Because it cannot incorporate a refractive atmosphere, the ray model would treat this case as equivalent to Base Case 1. Therefore, the HPM base case results could be thought to represent the ray model for this case.

Results of Case 3 deviate from Base Case 1 more substantially. While levels are similar between the two cases at the smaller ranges, severe drops in level are observed in Case 3 for the lowest three sources. This drop occurs when the receiver enters the shadow zone—regions into which rays cannot reach. A level decrease has also begun for the highest altitude source by 3 km range. However, ending propagation at 3 km prevents the shadow zone effect from fully materializing. For all sources, there is a slight increase in level just before the shadow zone, caused by the slight focusing of the remaining sound being directed upward.

The HPM and FFP results agree well after the smallest ranges and before the shadow zone has formed. Once levels drop below approximately 50 dB, the HPM and FFP results deviate slightly, with larger levels predicted by the HPM. These are the largest differences observed between the HPM and FFP models in the cases investigated. Their cause is unclear; however, the differences appear at levels that are low. A very small difference between HPM and FFP results in the opposite direction may have been expected from a range cutoff implemented in the PE model that is absent in the FFP. The cutoff in the PE stops propagation once levels drop below 120 dB from levels 1 m from the source for each frequency individually to save computation time. The FFP has no such cutoff built in and propagates each frequency of each condition to the full 3 km range.

Figure 8 shows a comparison of HPM results for the four source heights. When the full span of result levels is viewed, the cutoff of the PE propagation is seen clearly for the 40 m height source. For this source, results stop completely at 2840 m, before reaching the 3 km propagation range, indicating that results for all frequencies have satisfied the 120 dB down cutoff criteria. Additionally, slight downward stair steps can be seen in the levels of the 10, 40, and 100 m sources at the larger ranges, as the last frequencies stop propagating, one at a time. These numerical artifacts of the model implementation occur only when levels would be imperceptible to people and are not of concern. Because results are not returned for all source heights at the 3 km propagation range, overall levels at 2.5 m range are given: -34.8, -34.7, -17.6, and 54.2 dB for the 10 m, 40 m, 100 m, and 400 m sources, respectively. The spread in level among the four source heights at the range of 2.5 km is 89.0 dB. Case 3 shows, by far, the largest difference between results of the four source heights, for the propagation conditions explored in this report.

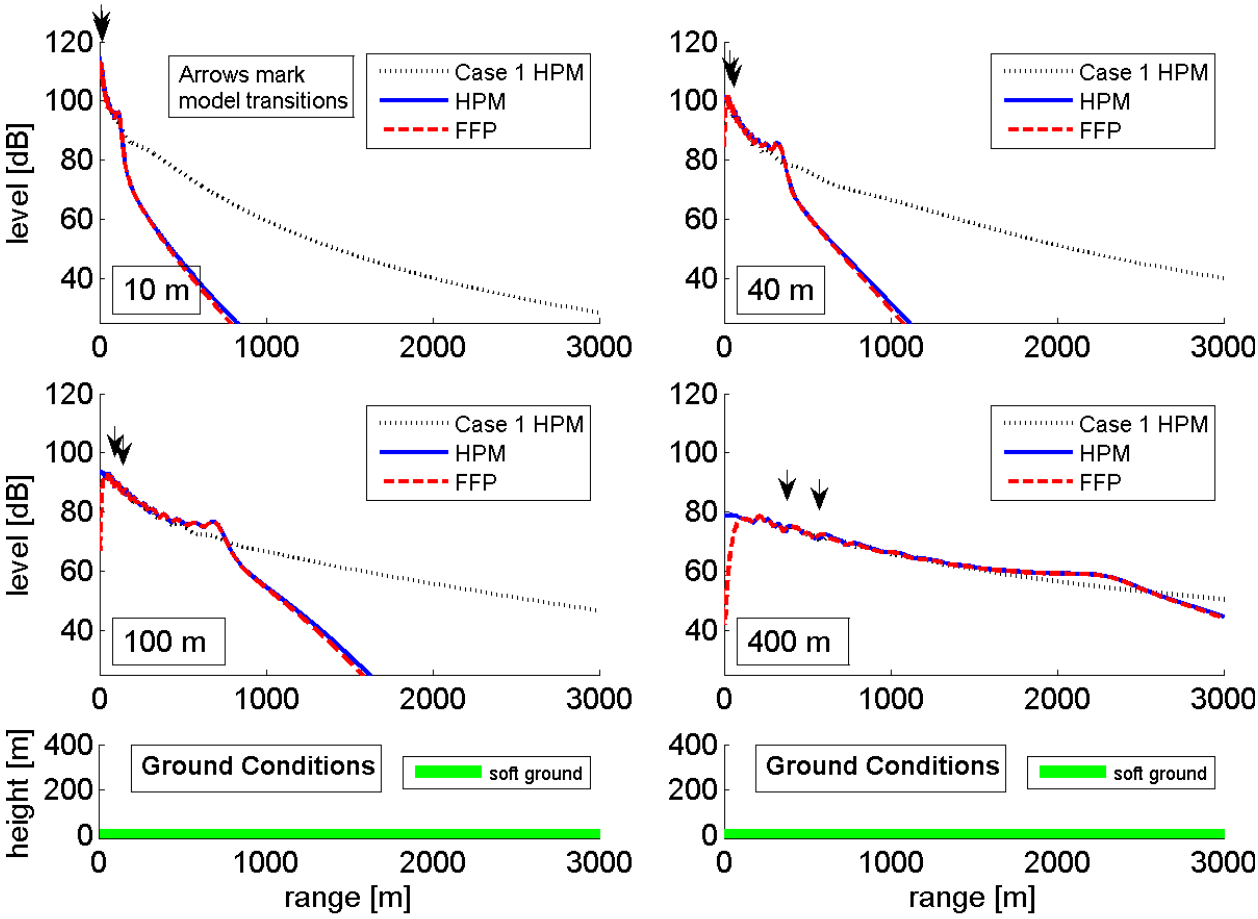

Figure 7. Case 3—Soft, flat ground and an upward refracting atmosphere. HPM and FFP results are compared for each source height—10 m, 40 m, 100 m, and 400 m. Results of the two models overlap over most of the range. Base Case 1 HPM results are included for comparison. A diagram of the propagation conditions is included beneath the results figures.

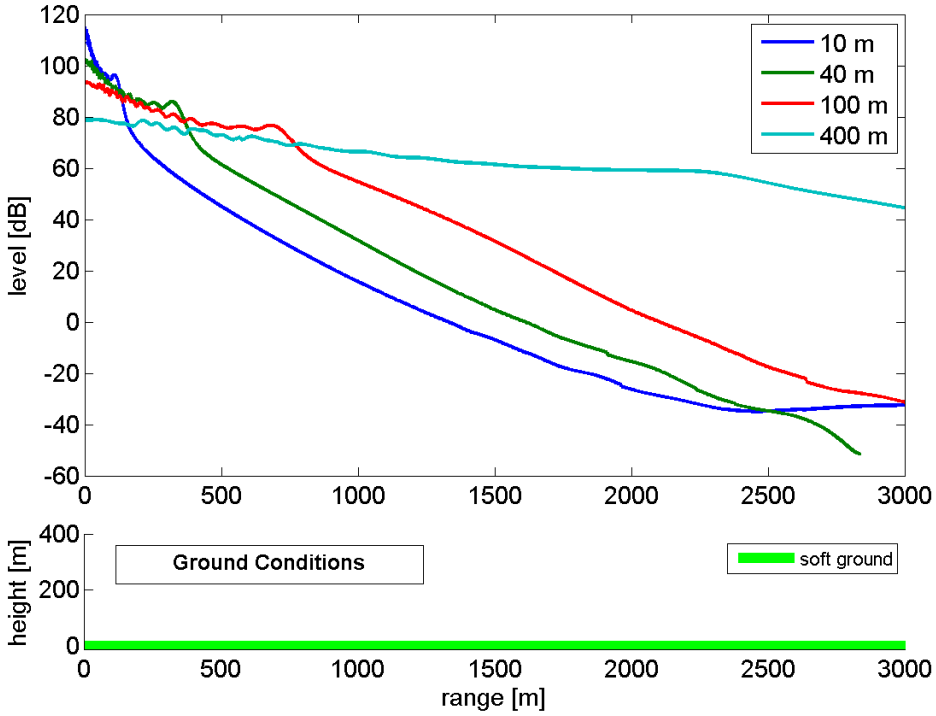

Figure 8. Case 3—Soft, flat ground and an upward refracting atmosphere. HPM results for each source height—10 m, 40 m, 100 m, and 400 m—plotted together. A diagram of the propagation conditions is included beneath the results figure.

4.4 Case 4: Soft, Flat Ground, Downward Refracting Atmosphere

The opposite of Case 3, Case 4 uses a downward refracting atmosphere with a logarithmic sound speed profile parameter of b = 1 m/s. A downward refracting atmosphere occurs in downwind conditions and during nighttime hours when the ground cools faster than the atmosphere and the temperature of the air increases with height above ground. Figure 9 shows the comparison between HPM and FFP results for each source height. The models again agree well beyond the smallest range values where the FFP is within 0.8, 0.2, 1.1, and 1.5 dB of the HPM for the 10, 40, 100, and 400 m sources, respectively, after the 200 m range. The downward refracting atmosphere results show lower levels than Base Case 1 at small ranges and higher levels than Base Case 1 at the longer ranges, for the lowest two source altitudes. Levels increase at larger ranges, where the sound has bent back toward the ground contributing to multiple ray arrivals. The effect of additional arrivals is seen in the jaggedness of results for the lowest altitude source. However, the downward refracting atmosphere has only a small effect on the results for the higher two source altitudes, which show slightly lower levels. This may be a result of investigating ranges too short to see the first additional arrival caused by refraction. At the horizontal propagation range of 3 km, the differences between Case 4 and 1 results are 19.0, 9.9, -0.7, and -1.5 dB for the 10, 40, 100, and 400 m source heights, respectively.

Figure 10 shows a comparison of HPM results for the four source heights. The results for the four sources are, again, more tightly grouped than in Base Case 1. In addition, the order of levels

for the sources is jumbled: the lowest level is reached by the 100 m source, then increasing in level, the 10 m, 400 m, and 40 m sources. The unordered nature of results is a consequence of the jagged pattern caused by additional ray arrivals. Overall levels at 3 km are 47.5, 50.0, 46.1, and 49.0 dB for the 10 m, 40 m, 100 m, and 400 m sources, respectively. The spread in level of among the four source heights at the 3 km range is 3.9 dB.

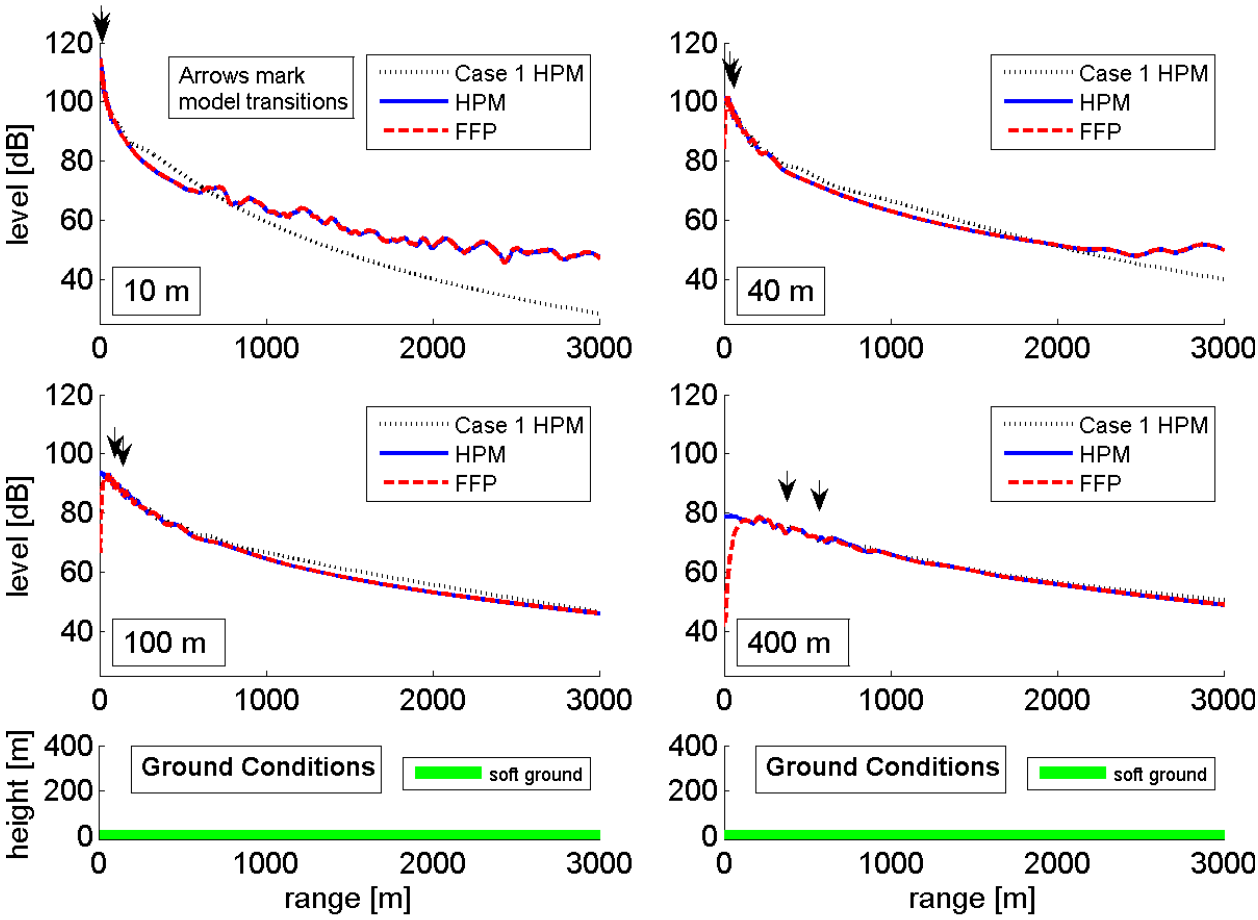

Figure 9. Case 4—Soft, flat ground and downward-refracting atmosphere. HPM and FFP results compared for each source height—10 m, 40 m, 100 m, and 400 m. Results of the two models overlap over most of the range. Base Case 1 HPM results are included for comparison. A diagram of the propagation conditions is included beneath the results figures.

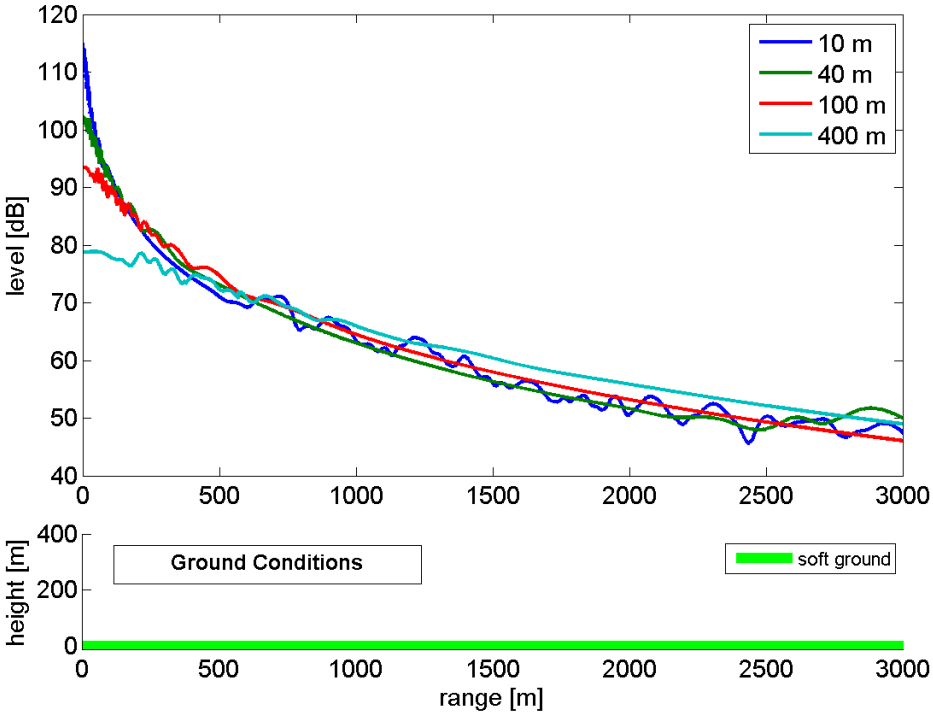

Figure 10. Case 4—Soft, flat ground and downward-refracting atmosphere. HPM results for each source height—10 m, 40 m, 100 m, and 400 m—plotted together. A diagram of the propagation conditions is included beneath the results figure.

4.5 Case 5: Soft Ground, Hill, Homogeneous Atmosphere

Case 5 introduces the effects of a terrain feature on propagation. Figure 11 shows the HPM results for propagation over a hill for each source height. The FFP and ray models are not included for comparison because neither incorporates range-dependent effects. However, Base Case 1 results are shown, which showed close agreement between the HPM, FFP and ray modeling in Section 4.1.

Because the model does not account for backscattering off obstacles, Case 5 results agree exactly with Base Case 1 until the horizontal range of 800 m, where the hill begins. For the three lowest sources, the level increases over the incline portion of the hill, as the sound interacts with the upslope. The increase is a fairly constant raise in level over the Base Case 1 results of between 9.48 and 13.4 dB for the lowest altitude source. The level remains within these increase bounds between the ranges of 863.0 and 1176 m, corresponding to slant distances between 863.0 and 1178 m and elevation angles between 0.3043 degrees below and 2.950 degrees above the horizontal of the source. Beyond the crest of the hill, where the line of sight between source and receiver is obstructed, there is a large drop in level. However, the level increases again over the end of the hill, and continues to increase into the second flat ground region, due to diffraction. The results level out toward the end of the 3 km propagation range, but never quite reach the larger levels of Base Case 1.

Results for the highest, 400 m altitude source agree well with Base Case 1, except over the downslope of the hill. Here, even though the line of sight between source and receiver is never fully broken, the direct ray passes very close to the ground. The reflected ray, therefore, meets the ground at a shallow angle, which can introduce a more significant ground effect than in the flat ground in Base Case 1. This effect could explain the small dip in Case 5 results for the 400 m source height over the downslope of the hill. At the horizontal propagation range of 3 km, the differences between Case 5 and 1 results are -13.2, -19.6, -12.6, and -0.4 dB for the 10, 40, 100, and 400 m source heights, respectively, demonstrating the large effect of the hill for all but the highest altitude source condition.

Figure 12 shows a comparison of HPM results for the four source heights. The trend in level is similar for the three lower source altitudes. The results for the four sources are, again, spread further than in Base Case 1: overall levels at 3 km are 15.3, 20.5, 34.1, and 50.0 dB for the 10, 40, 100, and 400 m sources, respectively. The spread in level among the four source heights at a range of 3 km is 34.7 dB. This is the third largest spread for the four sources, after Case 3, upward refracting atmosphere, and Case 6, upward sloping terrain, discussed in the next section.

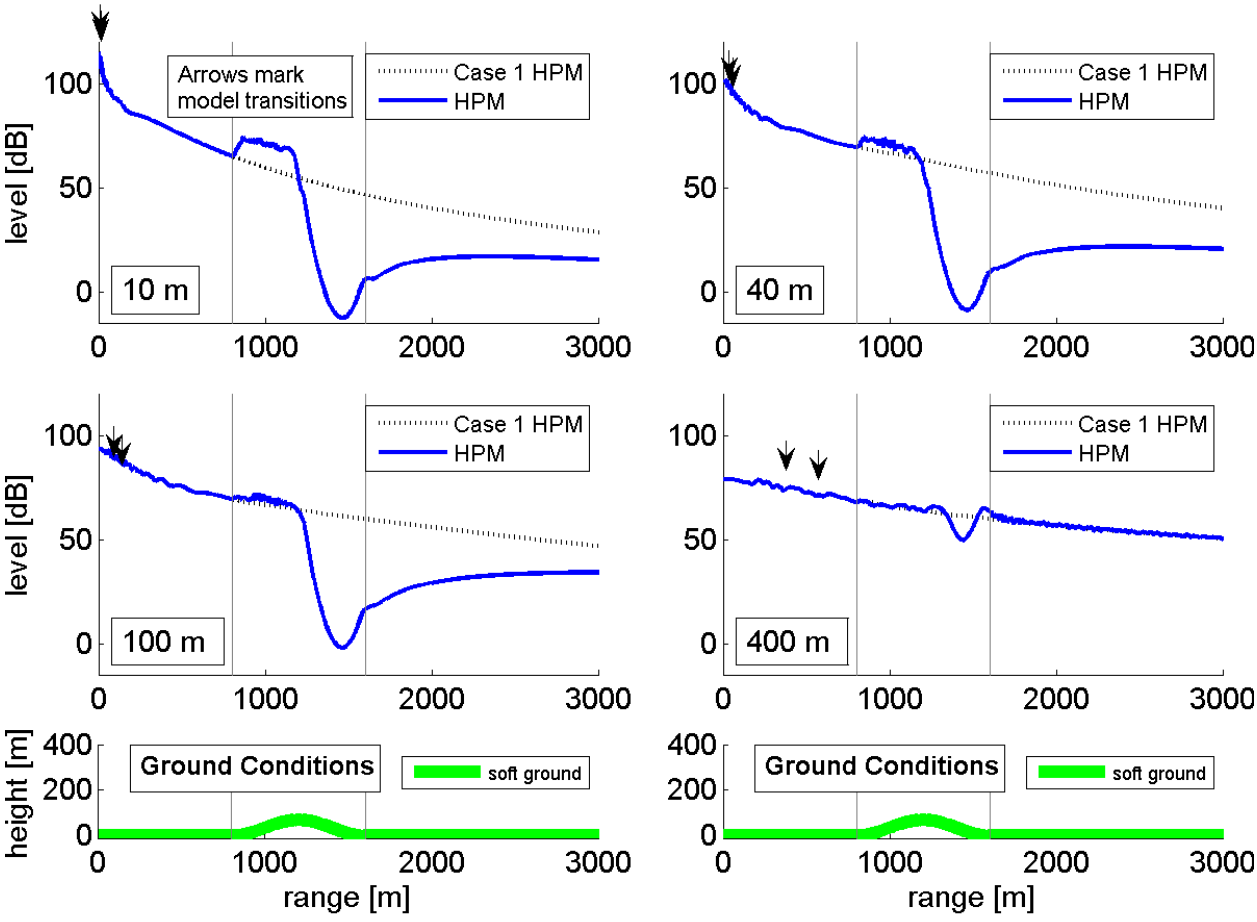

Figure 11. Case 5—Soft ground with hill terrain and homogeneous atmosphere. HPM results are shown for each source height—10 m, 40 m, 100 m, and 400 m. Case 1, baseline HPM results are included for comparison. A diagram of the propagation conditions is included beneath the results figures.

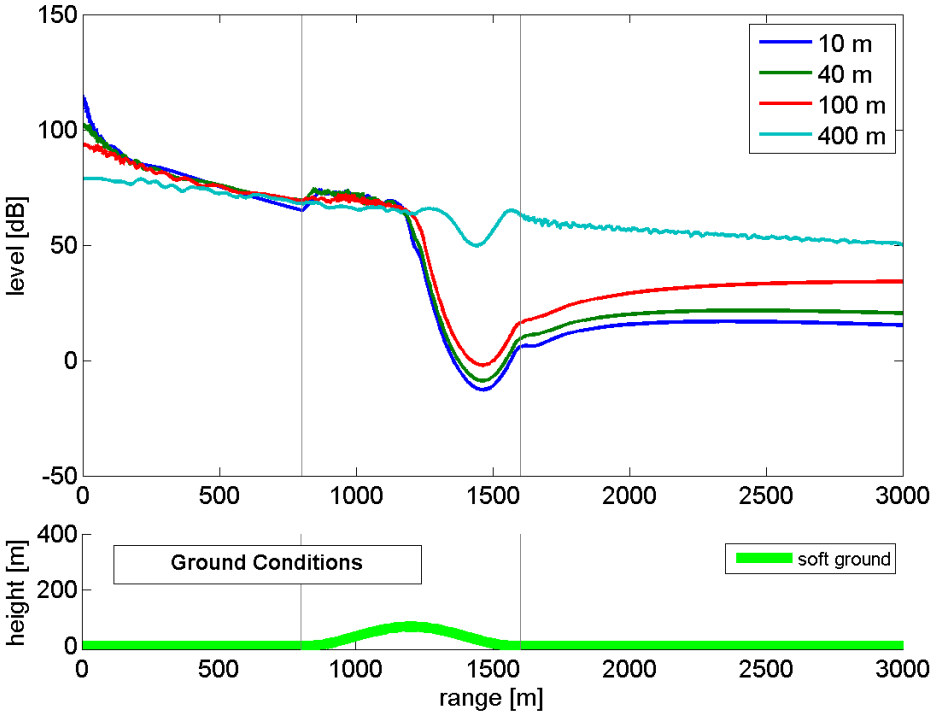

Figure 12. Case 5—Soft ground with hill terrain and homogeneous atmosphere. HPM results for each source height—10 m, 40 m, 100 m, and 400 m—plotted together. A diagram of the propagation conditions is included beneath the results figure.

4.6 Case 6: Soft Ground, Upward Sloping Terrain, Homogeneous Atmosphere

Case 6 represents an upward sloping terrain feature. Figure 13 shows the HPM results for each source height. Again, only the HPM results are presented in Figure 13 because this case includes range-dependent effects. However, both Base Case 1 and Case 5 results are included for comparison.

Because the propagation conditions of Case 6 are identical to those of Case 5 until the top of the upward slope at 1200 m range, the results of the two cases are equal to this point. Beyond the crest of the sloped ground, differences in results appear: (1) Unlike Case 5, a shadow zone formed by obstruction of the line of sight by the terrain feature only exists for the lower two source altitudes, rather than three. Furthermore, the shadow zones that are formed are less severe, reflected in the milder level decrease; and (2) Instead of the large dip, there are initial drops, with respect to Base Case 1, of approximately 11 to15 dB and 17 to20 dB for the 10 m and 40 m sources, respectively. These drops are maintained for the remainder of the propagation range.

Despite the absence of a line of sight blockage for the 100 m source, the upward sloping terrain does have an effect on results at larger ranges of propagation. An attenuation, which increases with increasing propagation range, is caused by an increase in ground effect. The shallower angle of reflection of the ray off the ground, due to the raised terrain, contributes to a ground

effect more similar to that of a 30 m altitude source over flat ground (100 m source height above the initial ground height, minus the 70 m ground height at and after 1200 m range), than of a 100 m altitude source.

The results of the 400 m source height, for which there is no line of sight blockage, and for which the angle of reflection of sound with the ground is still fairly steep, agree well with Base Case 1 over the full range.

Figure 14 shows a comparison of HPM results for the four source heights. Again, the results for the four sources are spread further than in Base Case 1 and the general trend is similar for the 3 lower source altitudes. Overall levels at 3 km are 13.2, 20.6, 37.9, and 50.4 dB for the 10, 40, 100, and 400 m sources, respectively. The spread in level among the four source heights at a range of 3 km is 37.2 dB. This is the second largest spread in results for the four sources, after Case 3, with an upward refracting atmosphere.

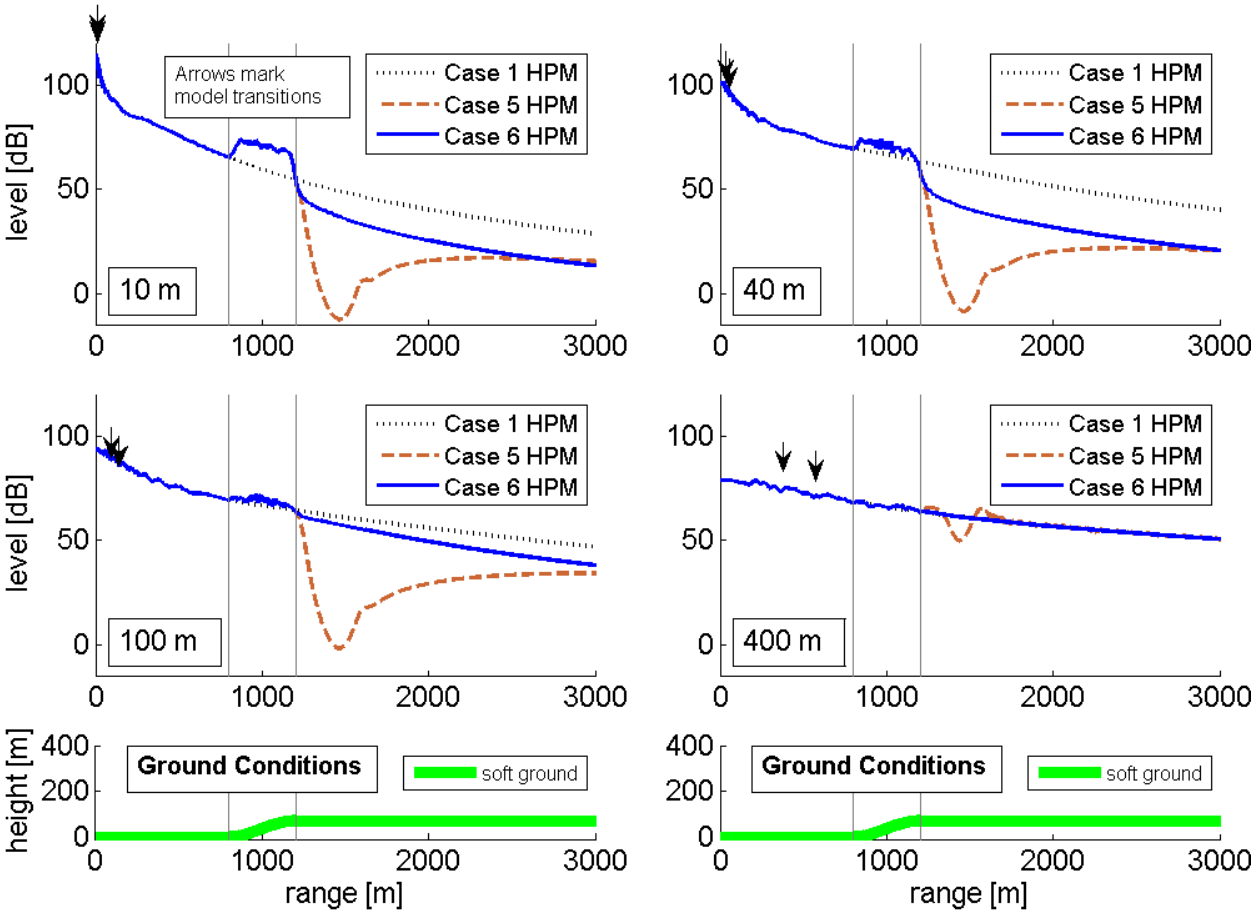

Figure 13. Case 6—Soft ground with upward sloping terrain and homogeneous atmosphere. HPM results are shown for each source height—10 m, 40 m, 100 m, and 400 m. Case 1, baseline HPM results are included for comparison. A diagram of the propagation conditions is included beneath the results figures.

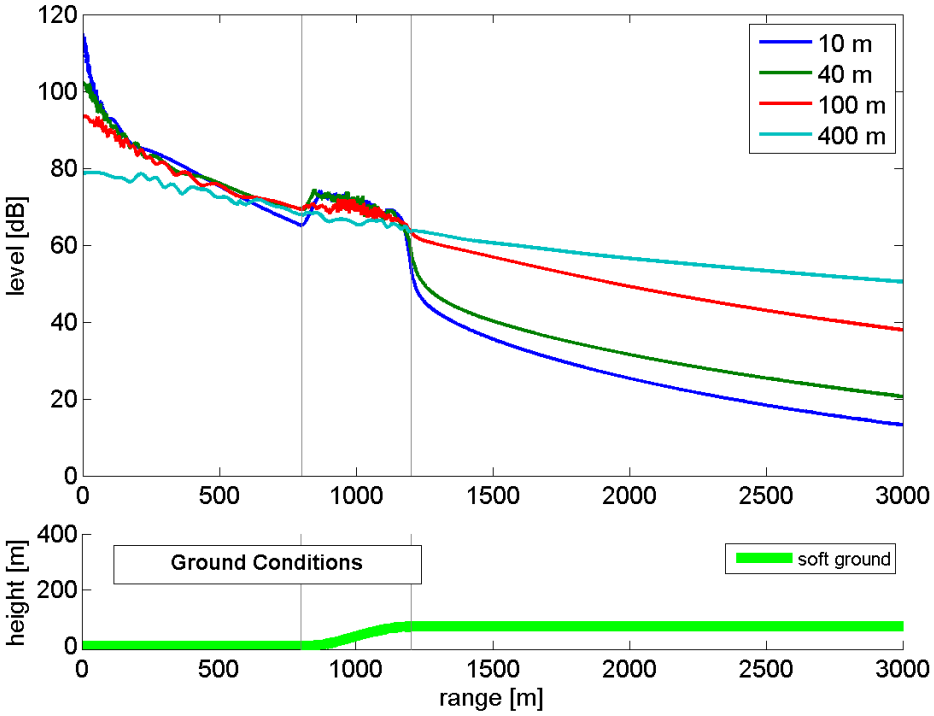

Figure 14. Case 6—Soft ground with upward sloping terrain and homogeneous atmosphere. HPM results for each source height—10 m, 40 m, 100 m, and 400 m—plotted together. A diagram of the propagation conditions is included beneath the results figure.

4.7 Case 7: Soft Ground, Downward Sloping Terrain, Homogeneous Atmosphere

Case 7 represents a downward sloping terrain feature. Figure 15 shows the HPM results for each source. Both Base Case 1 and Case 6 results are also included, for comparison. While the diagrams of the terrain conditions at the bottom of the figure indicate a higher terrain height at zero range, as measured against the absolute reference, the source heights are measured with respect to the ground directly underneath. Therefore, just as for Base Case 1, 10, 40, 100, and 400 m of vertical height exist between the sources and the ground, and Case 7 levels follow Base Case 1 until the start of the downslope at 800 m.

Dips in level, caused by a line of sight blockage, occur after the start of the downslope. The shapes of the dips resemble results for Case 5 beyond the peak of the hill, in Figure 11. However, the dips in Case 7 are not as extreme. In this case, the vertical height difference between the sources and receivers is larger because the sources were placed with respect to the raised terrain. The steeper elevation angles between sources and receivers cause a milder obstruction by the terrain feature. Furthermore, the downward slopes of Cases 5 and 7 begin at ranges of 1200 m and 800 m, respectively. The closer start of the downslope in Case 7 also contributes to a milder obstruction of the line of sight. Again, an increase in level caused by diffraction is observed over the end of the downslope, continuing over the flat ground.

In Cases 5 and 6, once the line of sight is broken by the hill or upward slope, respectively, the direct path is never recovered. In Case 7, there is a break in line of sight at 840, 858, and 895 m for the 10, 40, and 100 m sources, respectively. However, a direct path returns at 2207 and 1399 m, for the 40 and 100 m sources, respectively. Consequently, the 40 and 100 m source results reach, and then exceed, the levels of the Base Case 1 at longer ranges. The interesting effect causing levels to become larger than the Base Case 1 is the opposite of the effect causing lower levels for the 100 m source in Case 6. The higher altitude of the source with respect to receivers over the flat ground beyond the downslope creates a steeper angle of reflection off the ground. Therefore, the 40 m source acts more like a source at an altitude of 110 m over flat ground (40 m source height above the initial ground height, plus the 70 m ground height under the source), than of a 40 m altitude source. Because sound is reflected from the ground at a steeper angle, the ground effect is smaller and larger levels are observed. A small increase over Base Case 1 levels is also seen for the 100 m source. The effect, however, is negligible for the 400 m source.

Figure 16 shows a comparison of HPM results for the four source heights. Again, the general trend is similar for the 3 lower source altitudes. Overall levels at 3 km are 28.0, 47.6, 49.3, and 50.5 dB for the 10, 40, 100, and 400 m sources, respectively. The spread in level among the four source heights at a range of 3 km is 22.5 dB, similar to that of Base Case 1.

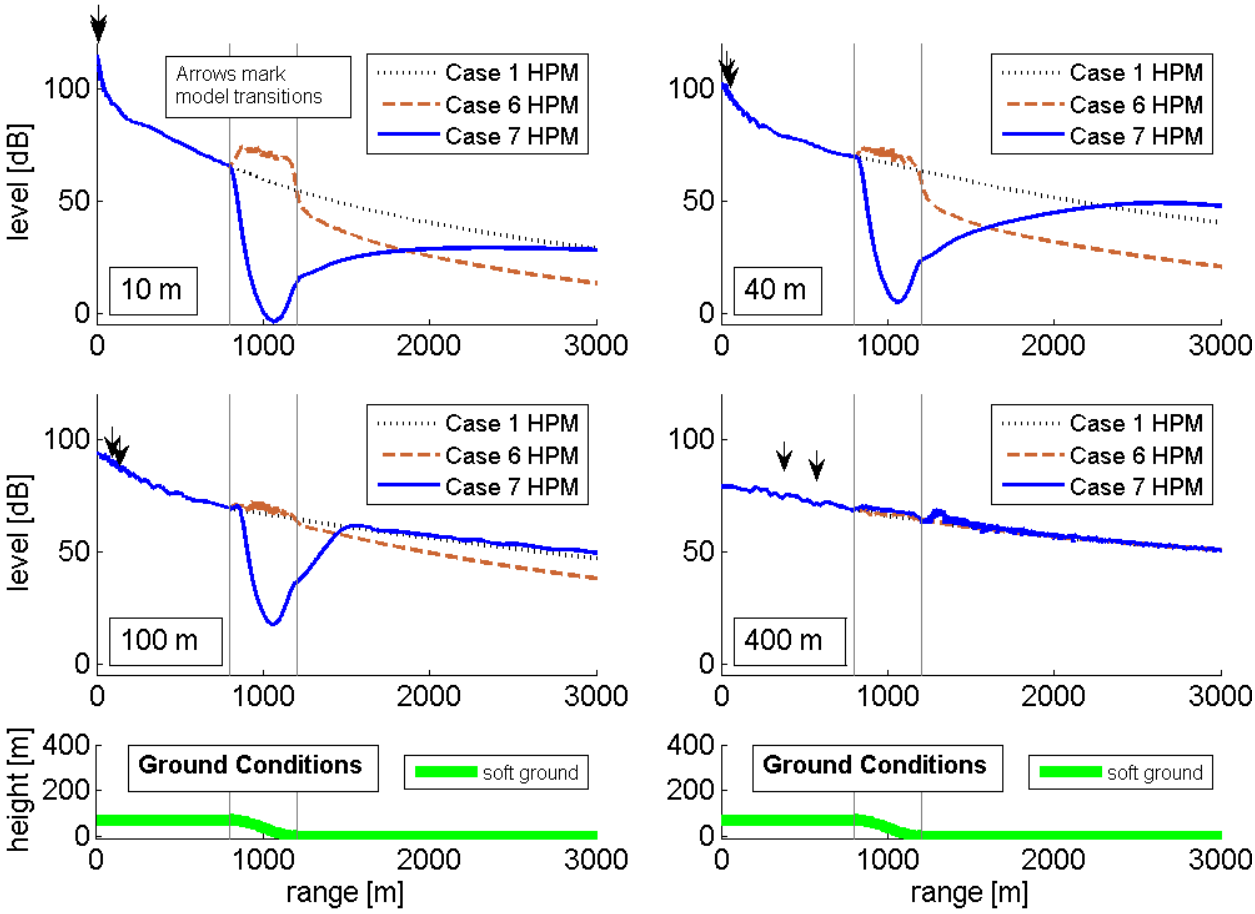

Figure 15. Case 7—Soft ground with downward sloping terrain and homogeneous atmosphere. HPM results are shown for each source height—10 m, 40 m, 100 m, and 400 m. Case 1, baseline HPM results are included for comparison. A diagram of the propagation conditions is included beneath the results figures.

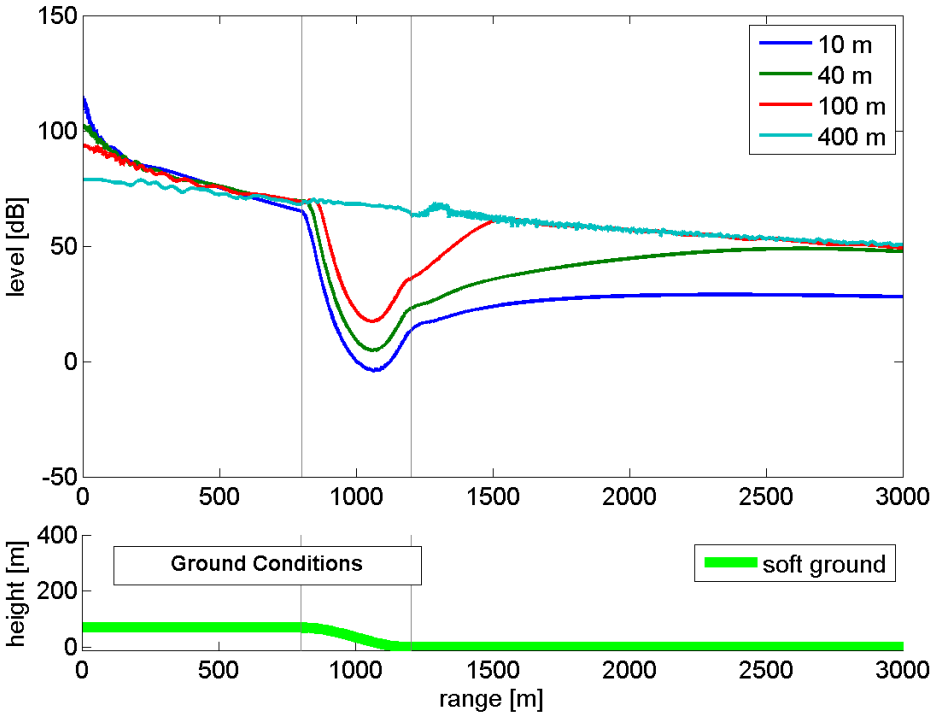

Figure 16. Case 7—Soft ground with downward sloping terrain and homogeneous atmosphere. HPM results for each source height—10 m, 40 m, 100 m, and 400 m—plotted together. A diagram of the propagation conditions is included beneath the results figure.

4.8 Case 8: Hard to Soft Ground, Flat Terrain, Homogeneous Atmosphere

Case 8 considers the effect of transitions between ground types. Figure 17 shows the HPM results for a transition from hard to soft ground for each source height. In this figure, both the Base Case 1, with soft ground, and Case 2, with hard ground, are included for comparison. However, again, because propagation effect of the ground type transition is range-dependent, neither FFP or ray results are included.

Case 8 results are equal to results of Case 2 at the smaller ranges where propagation is over hard ground. At the transition to soft ground, results diverge from the Case 2, hard ground results, and approach Base Case 1, soft ground, results. For the lowest altitude source at 10 m height, the Case 8 results at the farthest point of propagation are approximately 1.8 dB higher than Base Case 1, soft ground results. However, for the 3 highest altitude source, Base Case 1 and Case 8 results are nearly equal at 3 km range.

Figure 18 shows a comparison of HPM results for the four source heights. The results for the four sources resemble those of Base Case 1: overall levels at 3 km are 30.3 dB, 40.1 dB, 46.7 dB, and 50.4 dB for the 10 m, 40 m, 100 m, and 400 m sources, respectively. There is a spread in level of 20.1 dB among the four source heights at a range of 3 km.

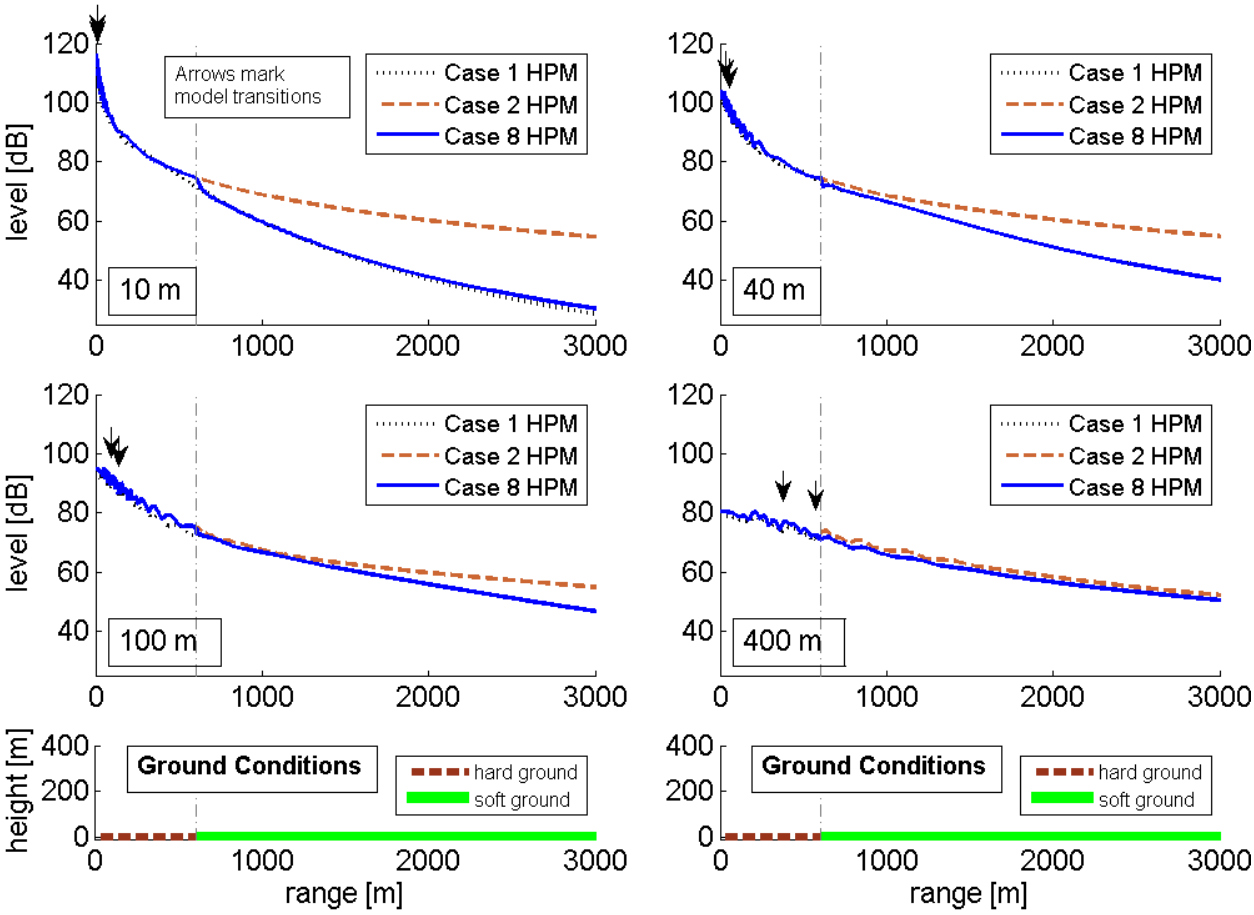

Figure 17. Case 8—Hard to soft ground transition with flat terrain and homogeneous atmosphere. HPM results are shown for each source height—10 m, 40 m, 100 m, and 400 m. Baseline Case 1 and Case 2 HPM results are included for comparison. A diagram of the propagation conditions is included beneath the results figures.

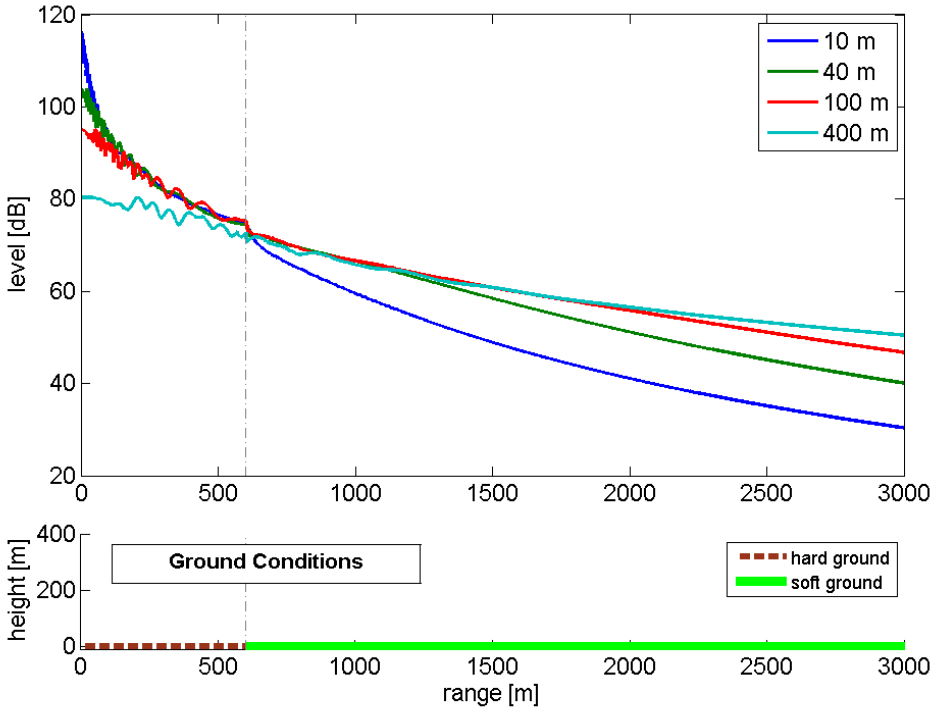

Figure 18. Case 8—Hard to soft ground transition with flat terrain and homogeneous atmosphere. HPM results for each source height—10 m, 40 m, 100 m, and 400 m—plotted together. A diagram of the propagation conditions is included beneath the results figure.

4.9 Case 9: Soft to Hard Ground, Flat Terrain, Homogeneous Atmosphere

Case 9, the opposite of Case 8, considers the effect of a transition from soft to hard ground. Figure 19 shows the HPM results for each source. Again, both Base Case 1, soft ground, and Case 2, hard ground, are included for comparison.

A similar, though opposite pattern is seen in Case 9, as compared with Case 8. Here, the results of propagation at the beginning ranges over soft ground are equal to those of Base Case 1. At the transition to hard ground at the 600 m range, the results diverge from Base Case 1 results and approach results of Case 2. Again, results for the lowest source do not quite reach the results for a purely hard ground, but are lower by approximately 2.4 dB at 3 km range. However, for the 3 highest altitude source, Cases 1 and 9 are nearly equal at 3 km range.

Figure 20 shows a comparison of HPM results for the four source heights. The results for the four sources resemble those of Case 2: overall levels at 3 km are 52.2, 54.9, 54.7, and 52.2 dB for the 10 m, 40 m, 100 m, and 400 m sources, respectively. There is a spread in level of only 2.8 dB among the four source heights at the 3 km range.

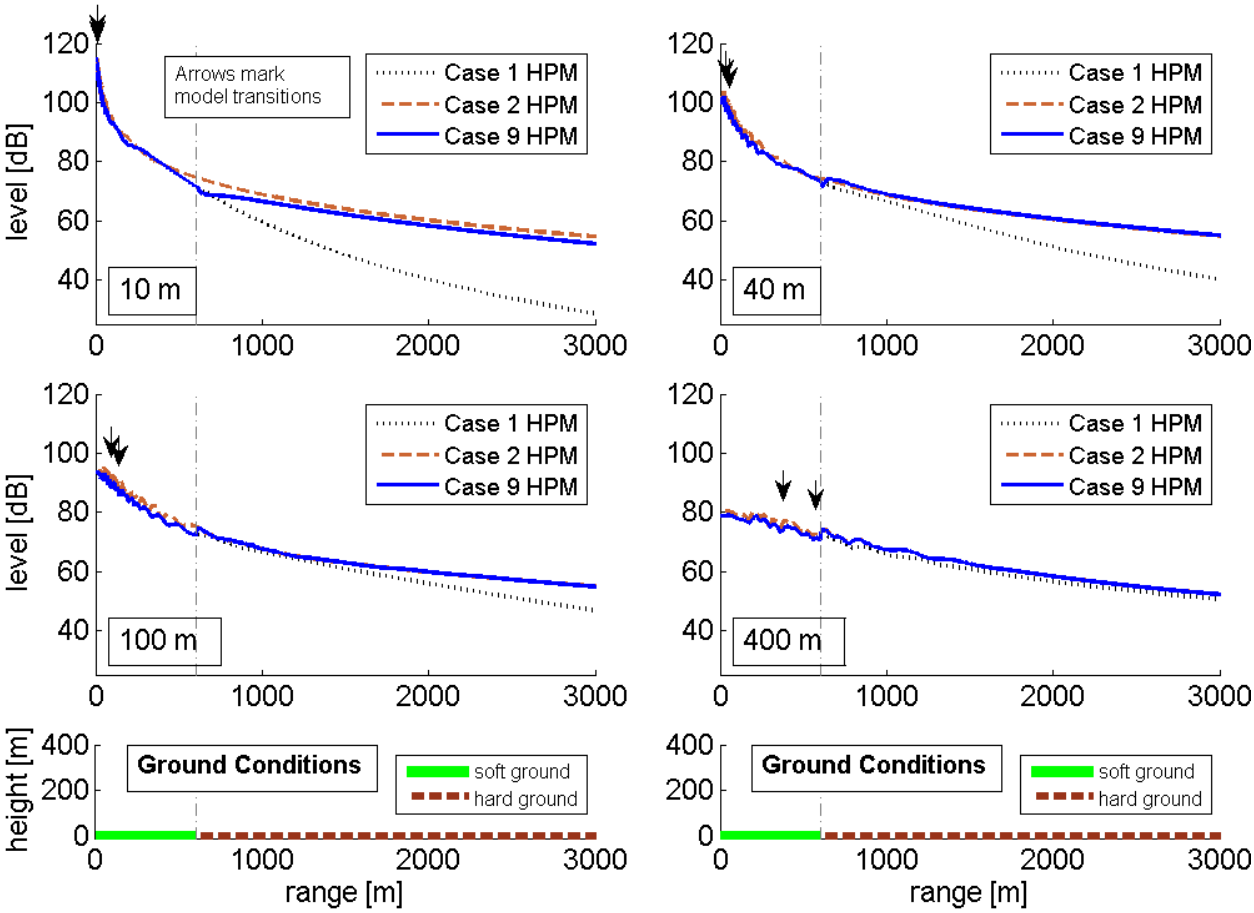

Figure 19. Case 9—Soft to hard ground transition with flat terrain and homogeneous atmosphere. HPM results are shown for each source height—10 m, 40 m, 100 m, and 400 m. Base Case 1 and Case 2 HPM results are included for comparison. A diagram of the propagation conditions is included beneath the results figure.

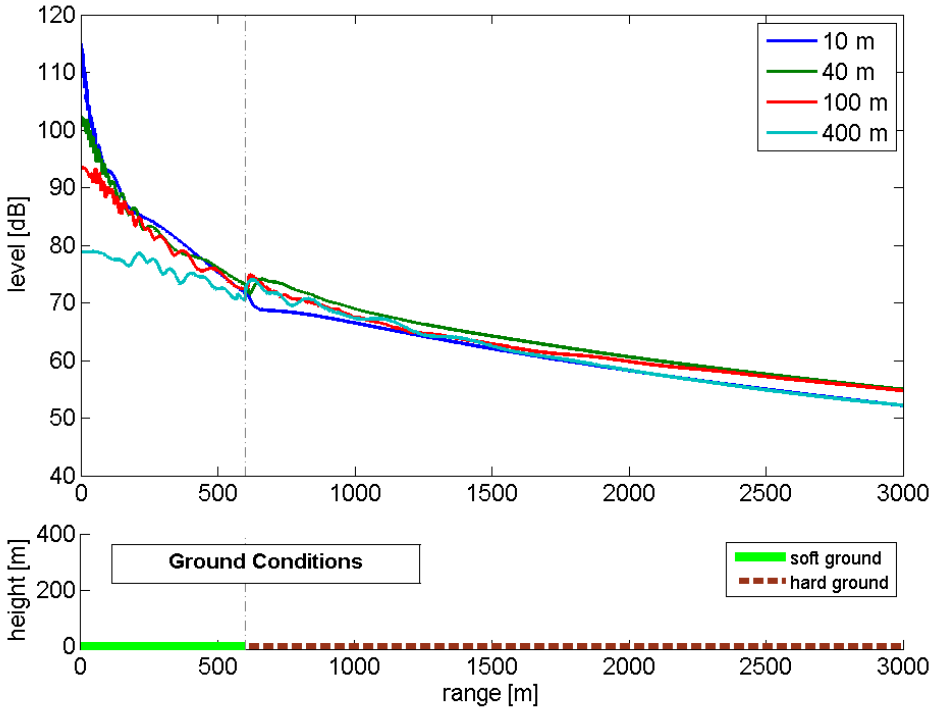

Figure 20. Case 9—Soft to hard ground transition with flat terrain and homogeneous atmosphere. HPM results for each source height—10 m, 40 m, 100 m, and 400 m—plotted together. A diagram of the propagation conditions is included beneath the results figures.

4.10 Case 10: Hard to Soft to Hard Ground, Flat Terrain, Homogeneous Atmosphere

Case 10 combines two ground type transitions, from hard to soft ground at 600 m, and then back to hard ground at 1800 m. Figure 21 shows the HPM results for each source. Results from cases 1 and 2 are included for comparison.

The results of Case 10 are equal to Case 8, hard to soft ground, before the second ground type transition at 1800 m range. After the second transition, from soft to hard ground, levels increase and approach Case 2. The 10 m source levels do not quite reach Case 2 levels within the 3 km propagation range, with a difference of -8.9 dB between Cases 10 and 2. However, the three higher altitude sources do, approximately, reach the Case 2 levels, with differences between Case 10 and 2 results equaling 0.8, 0.2, and -0.0 dB for 40, 100, and 400 m source altitudes, respectively.

Figure 22 shows a comparison of HPM results for the four source heights. The results for the four sources resemble those of the Case 2: overall levels at 3 km are 45.6 dB, 55.5 dB, 55.0 dB, and 52.2 dB for the 10 m, 40 m, 100 m, and 400 m sources, respectively. There is a spread in level of 9.9 dB among the four source heights at a range of 3 km.

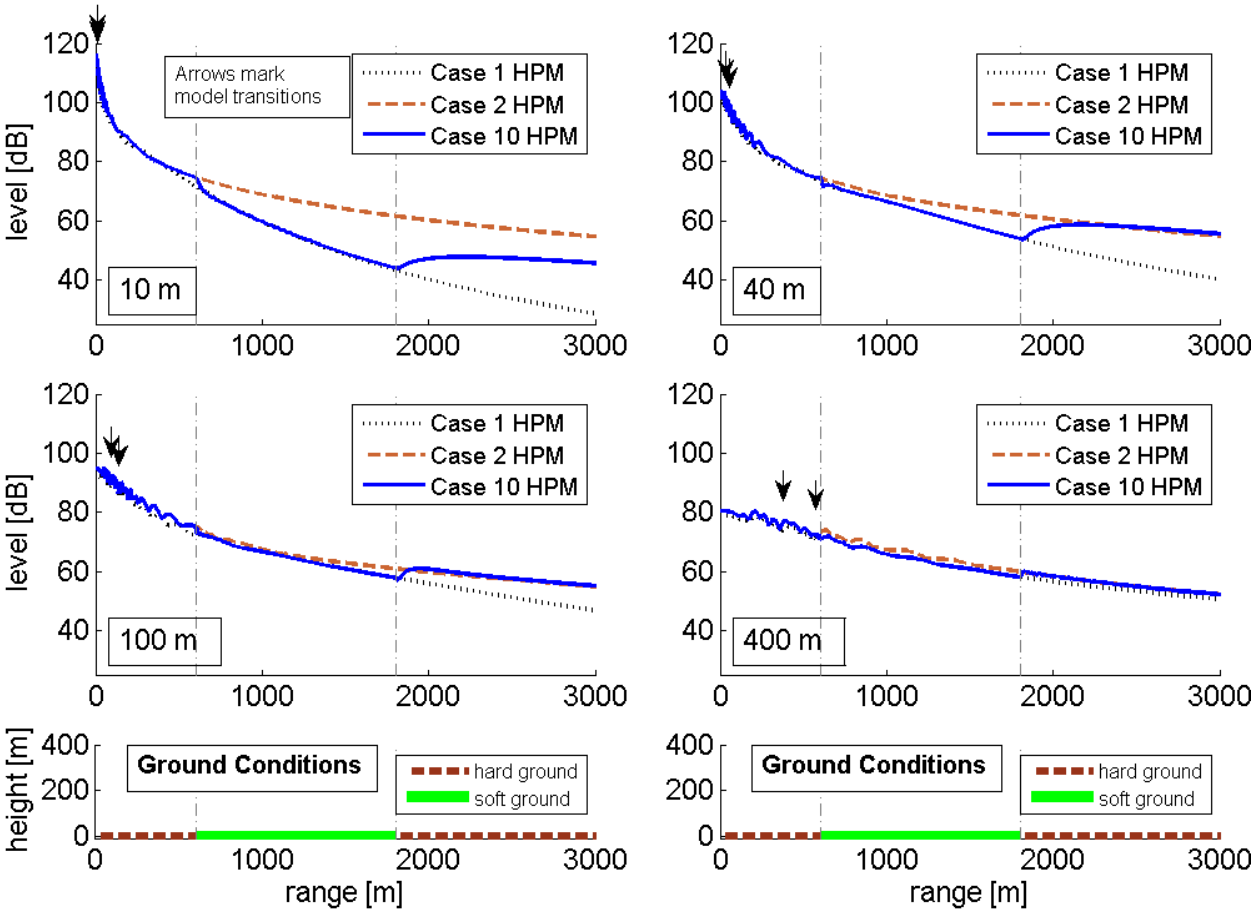

Figure 21. Case 10—Hard to soft to hard ground transitions with flat terrain and homogeneous atmosphere. HPM results are shown for each source height—10 m, 40 m, 100 m, and 400 m. Base Case 1 and Case 2 HPM results are included for comparison. A diagram of the propagation conditions is included beneath the results figures.

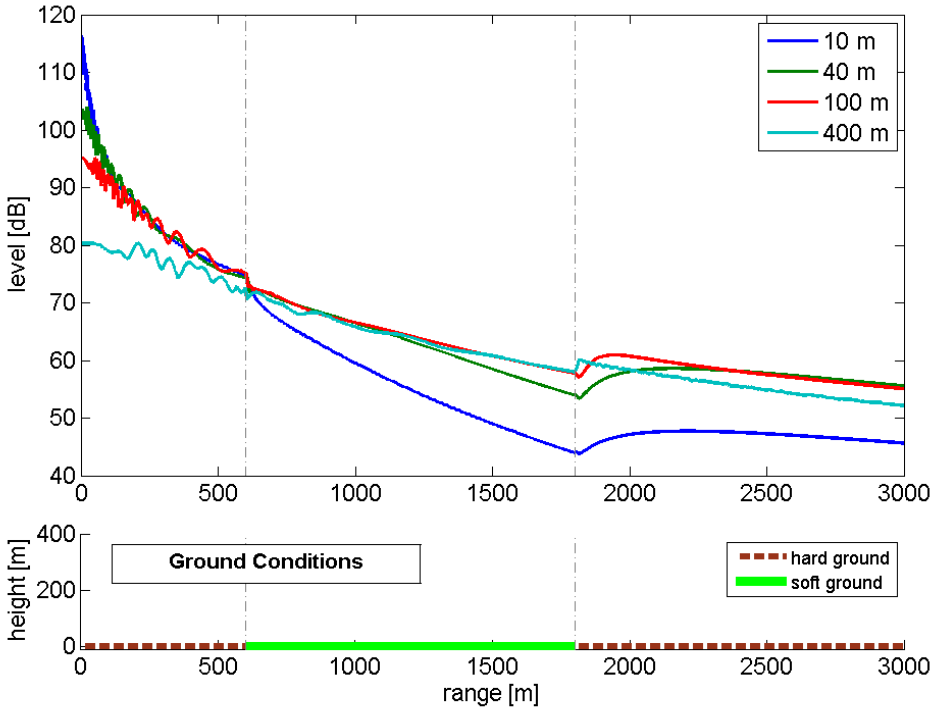

Figure 22. Case 10—Hard to soft to hard ground transitions with flat terrain and homogeneous atmosphere. HPM results for each source height—10 m, 40 m, 100 m, and 400 m—plotted together. A diagram of the propagation conditions is included beneath the results figure.

4.11 Case 11: Hard to Soft to Hard Ground, Hill, Downward Refracting Atmosphere

Case 11 represents a more realistic combination of propagation effects, including ground type transitions from hard to soft to hard ground, a hill feature, and a downward refracting atmosphere. Therefore, all three of the types of propagation mechanisms explored in this report are addressed in this single case. Figure 23 shows a comparison of HPM results for the four source heights. Along with Base Case 1 results, the Case 4 (downward refracting atmosphere), Case 5 (hill terrain), and Case 10 (transition from hard to soft to hard ground) results are also included for comparison.

In Case 11, the interaction of the different propagation mechanisms is significant for the three lowest altitude sources. For example, the lowest, 10 m source shows the largest impact of the shadow zone behind the hill, under Case 5 conditions (Figure 11). In addition, the downward refracting atmosphere of Case 4 has the highest impact for the 10 m source (Figure 9). Because the downward refracting atmosphere helps to fill in the shadow zone created by the hill by offsetting the line of sight blockage, Case 11 results show closer agreement with Base Case 1 in the shadow zone region over the downslope of the hill. In the smaller ranges of propagation before range-dependent effects begin (from approximately 200 to 600 m), the downward refractive atmosphere is seen to reduce levels. Therefore, the Case 11 results in this region fall

between the lower downward refractive atmosphere results and the higher results of the homogeneous atmosphere cases. Finally, at the end of the propagation range of 3 km, Case 11 results are approximately equal to the hard-to-soft-to-hard ground transition (Case 10) results, which share its ground type. Case 11 results are also slightly lower than the downward refractive atmosphere (Case 4) results, and significantly higher than the base case and hill case results (Cases 1 and 5) by 17.3 and 30.5 dB, respectively.

The changing relationship between Case 11 results and those of Cases 1, 4, 5, and 10 for the 10 m source over the full range of propagation indicates the complicated interaction of effects. It is not always easy to predict which effect may be dominant in a given propagation region; the isolated mechanism case with which Case 11 results agree most closely changes across the 3 km range.

Many similarities in pattern are seen for the middle altitude, 40 and 100 m height, sources. For both the 40 and 100 m sources, like the 10 m source, the shadow zone behind the hill is filled in by the downward refracting atmosphere. However, for the 40 and 100 m sources, the levels at 3 km horizontal range fall closer to those of Cases 1 and 4, the base case and downward refracting atmosphere case, respectively, rather than Case 10 (the hard-to-soft-to-hard ground transition case), which records larger levels.

Finally, results for the 400 m source are similar to those of Case 10, depending primarily on the impedance of the ground under the receiver. Again, under these source conditions, the line of sight is never broken and the downward refracting atmosphere is not needed to fill in dips in level. Still, the effect of the hill is seen in the small peaks in level near the top and end of the hill. These are similar to the small peaks in level seen in Case 5, which border its dip in level. However, the dip has been filled in Case 11.

Figure 24 shows a comparison of HPM results for the four source heights. Overall levels at 3 km are 45.8, 45.2, 47.2, and 50.6 dB for the 10 m, 40 m, 100 m, and 400 m sources, respectively. There is a spread in level of only 5.4 dB among the four source heights at a range of 3 km. The patterns of Case 11 results can be seen to be more complex than the results of the isolated mechanism cases.

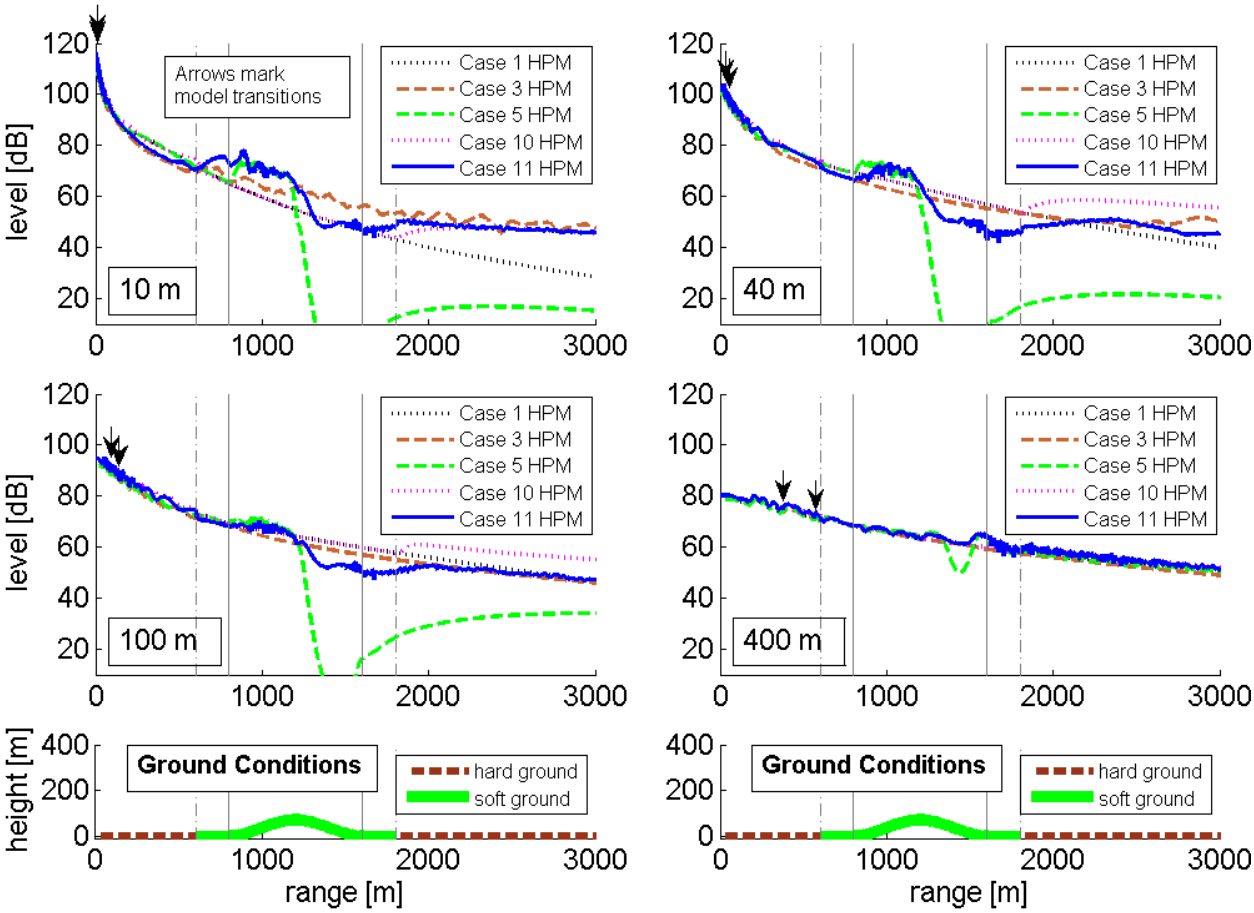

Figure 23. Case 11—Hard to soft to hard ground transitions with hill terrain and downward-refracting atmosphere. HPM results are shown for each source height—10 m, 40 m, 100 m, and 400 m. Base Case 1 HPM results are included for comparison. A diagram of the propagation conditions is included beneath the results figures.

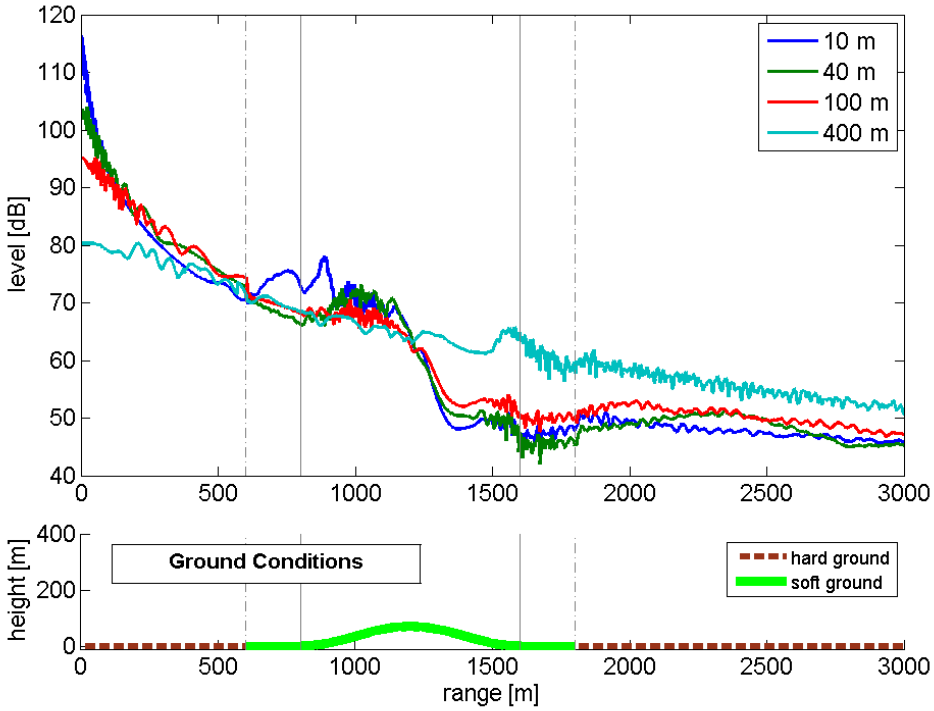

Figure 24. Case 11— Hard to soft to hard ground transitions with hill terrain and downward-refracting atmosphere. HPM results for each source height—10 m, 40 m, 100 m, and 400 m—plotted together. A diagram of the propagation conditions is included beneath the results figure.

5. FURTHER ANALYSIS

The comparisons between the results of the eleven different cases discussed in this report help determine where a detailed propagation model is necessary to capture all significant effects, and where a simpler model may be sufficient. All three models—HPM, FFP, and ray—were found to return nearly equivalent results for the simplest propagation conditions in Cases 1 and 2. The agreement of the three HPM component models under these conditions not only provide further confirmation of the correctness of the model implementations, as checks against each other, but also justifies utilization of the "intelligent switching" concept, by which component models may be chosen as surrogates for the full HPM in order to reduce runtimes. If such a protocol could be developed that has negligible impact on the accuracy of the noise level predictions, it would move the HPM a step closer to integration into the AEDT. As an example, Base Case 1 took over two days to run with the HPM and slightly under two days to run with just the FFP. In contrast, the ray model ran Base Case 1 in less than a minute. Such a large decrease in runtime is extremely valuable. Still, the ray model is slower than the INM, which takes only seconds to run. Cases 1 and 2 provide proof of concept that at least two sets of propagation conditions are ideal candidates for a "switch" to use of the ray model in place of the full HPM.

Nine additional cases were run to explore the capabilities of the HPM and to provide further investigation into the intelligent switching strategy. In running these cases, some preliminary insights were gained regarding both the conditions under which a simpler component model might be substituted for the HPM, as well as conditions for which the full HPM incorporates important effects that the simpler models are unable to capture:

Case 3, Soft, Flat Ground, Upward Refracting Atmosphere. Case 3 underscores the scale of effects certain propagation mechanisms can have on overall reported levels. In this case, not only were large drops in level observed inside shadow zone regions, but small increases in level were detected before the start of the shadow zone. However, while inaccurate results would be returned by a model incapable of including atmospheric effects, such as our straight-ray model, the FFP shows fairly good agreement with the full HPM results, especially in the beginning portion of the shadow zone, where levels are decreased, but still likely audible. Thus, Case 3 suggests that, for an upward refracting atmosphere, care must be taken inside a shadow zone, and in the region in front of a shadow zone. The FFP can be used in place of the full HPM to save a small amount of runtime.

Case 4, Soft, Flat Ground, Downward Refracting Atmosphere. In conditions of a downward refracting atmosphere, multiple arrivals from sound reflected off the ground more than once cause increased levels at larger horizontal propagation ranges. This is especially noticeable for low altitude sources. Similar, though opposite to upward refracting atmosphere conditions, the region in front of the area showing the most obvious effect of the atmosphere is also impacted. In Case 4, a region of decreased levels is formed in front of the region of increased level. Results for the highest altitude source indicate that these effects may become fairly small for high altitude sources. However, it is possible that they would appear if the propagation range was extended. Thus, Case 4 suggests that care must be taken at ranges that support more than two (direct and single reflection) paths from source to receiver, as well as the region in front of them. Again, the FFP can be used in place of the full HPM to save a small amount of runtime.

Case 5, Soft Ground, Hill, Homogeneous Atmosphere. Case 5 clearly demonstrates the effect of a line of sight blockage between a source and receiver. A large drop in level is observed following the initial obstruction of the direct path, while diffraction increases the attenuated levels both over the end of the terrain feature and into the flat region beyond. In addition, there is an increase in level over the inclined portion of terrain for the lower altitude sources. While the absence of line of sight blockage for the highest altitude source does cause levels to show little effect of the terrain feature for the majority of the propagation range, an effect of shallow angle of reflection off the ground causes a small dip in level over the back of the hill. Thus, Case 5 suggests that, when the dimension of the terrain feature are small compared to the source altitude, and the line of sight between source and receiver is not broken, the effect of a terrain feature is greatly diminished. Because the ray model, FFP, and HPM results all agree for simple propagation conditions like Base Case 1, and because the hill case results for the high altitude source agree well with Base Case 1 results, a switch from the full HPM to one of the simpler models could be employed. However, if a simpler propagation method, such as the straight-ray model, is to be substituted for the full HPM, care must also be taken to ensure a minimum steepness of the sound reflected off the ground at all points in range. If differences between the full HPM and the simple ray model do exist, they would be seen near the terrain feature.

Case 6, Soft Ground, Upward Sloping Terrain, Homogeneous Atmosphere. Case 6 reinforces the lessons of line of sight blockage introduced in Case 5. It also further supports the need for attention to the angle of reflection of sound off the ground. Here again, the shallower angle of reflection off the ground, in this case due to raised terrain rather than the terrain slope, causes increased ground effect and attenuations in level. However, the highest altitude source in Case 6 provides an excellent example of conditions under which the straight-ray model could be substituted for the full HPM with negligible impact on overall noise level predictions.

Case 7, Soft Ground, Downward Sloping Terrain, Homogeneous Atmosphere. Case 7 reinforces the lessons of Case 5 and 6, in terms of line of sight blockage and reflection angle off the ground. Here, the opposite effect of changing the angle of reflection was observed: the angle of reflection became steeper over the sunken terrain than it would have been over a completely flat ground. Therefore, there was an increase in level above Base Case 1. Although there was an unexpected, small increase in level over the downward slope and another just following the end of the downslope for the highest source altitude condition, Case 7 also suggests that the straight-ray method may be a candidate for modeling propagation for a high altitude source over a downward sloping ground. However, Case 7 results were not as convincing as those of Case 6 and, therefore, caution should be used in predicting levels in regions near the terrain feature.

Cases 8, 9 and 10, Hard to Soft Ground, Soft to Hard Ground, and Hard to Soft to Hard Ground, Flat Terrain, Homogeneous Atmosphere. The cases of propagation over transitions between different types of ground reveal a few points of caution and also a few instances of support for intelligent switching. In these cases, it was found that the effect of a transition of ground type can be significant for a low altitude source out to long ranges. However, for fairly high altitude sources, the effect of the previous ground type on the results at a receiver placed after the transition does not last long. This suggests that, if the receiver is far enough from the transition point, a single ground impedance input reflecting the type of ground directly beneath the receiver is sufficient. Thus, for high altitude sources for which angles of ground reflections are steep enough, the straight-ray model can be substituted for the full HPM at most points in range.

Case 11, Downward Refracting Atmosphere, Hill Terrain, and Hard to Soft to Hard Ground. Results of this case serve to reinforce the complexity of interactions between different propagation mechanisms. It is clear that attempts to determine the total effect of all propagation mechanisms from the effects of the isolated mechanisms alone would not be recommended. However, results for the highest altitude source do increase support for an intelligent switching scheme: the 400 m height source results are similar to those of Case 10, especially in regions beyond the terrain feature. This indicates that a simpler model could be substituted for the full HPM for high altitude sources. Figure 25 shows a plot of the highest altitude source for all 11 cases used in this report. This figure is presented to give a better illustration of the similarities of the results for the source across varied propagation conditions. Some deviations from the group can be seen, for example, in the refractive atmosphere Cases 3 and 4 at the longer ranges, and in Case 5 results just beyond the peak of the hill. However, excluding Case 3, the results have a group span in level of only about 3 dB over the full range of propagation. It can also be seen that the grouping of results tightens toward the longer ranges. Figure 26 shows a portion of Figure 25, zoomed in at the longer ranges. Here a grouping between cases 1, 5, 6, 7, and 8, and between Cases 2, 9, 10, and 11 is seen even more clearly. The first group, at the lower levels, is the homogeneous atmosphere cases with propagation over all or mostly soft ground. The second group, at the higher levels, is the homogeneous atmosphere cases with propagation over all or mostly hard ground. Within these groups, results deviate by less than 1 dB. Finally, the two outliers are the refractive atmosphere cases, Cases 3 and 4. Still there is less than a 1.5 dB difference between Cases 1 and 4, and less than a 6 dB difference between Cases 1 and 3.

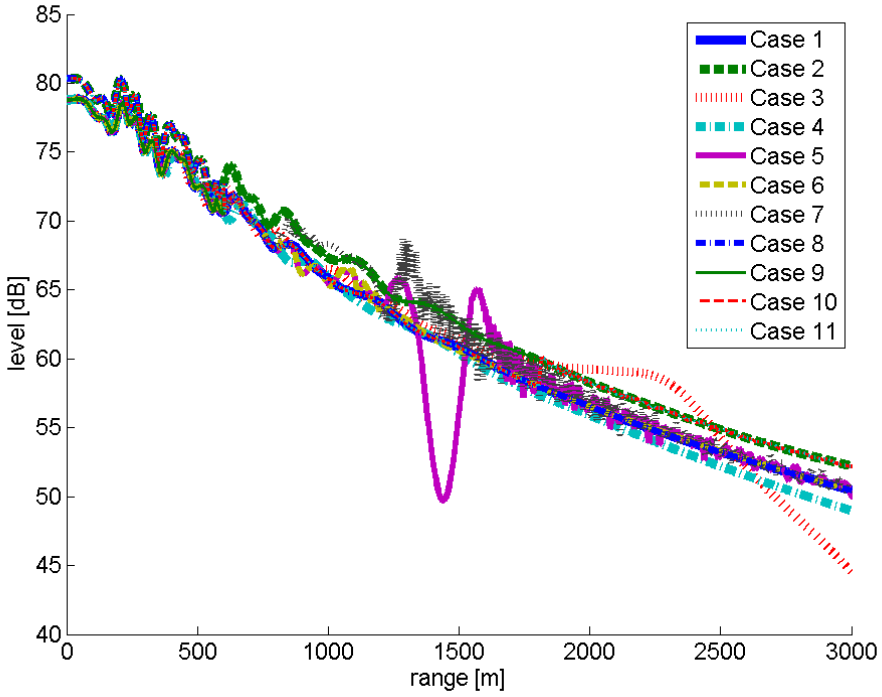

Figure 25. Results for the highest altitude (400 m high) source. All cases plotted together.

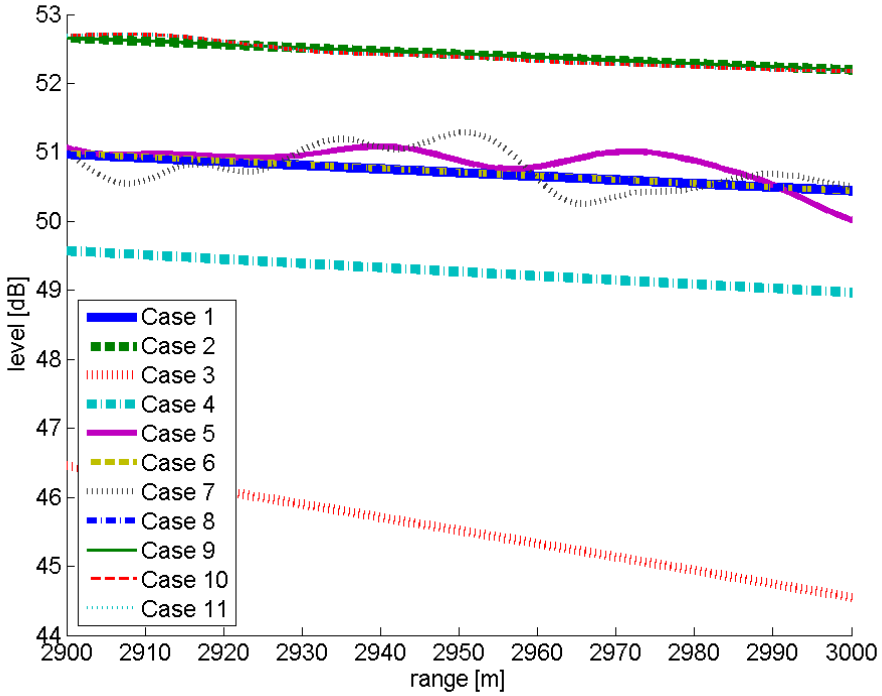

Figure 26. Results for the highest altitude (400 m high) source - zoomed in view at longer ranges. All cases plotted together.

6. CONCLUSIONS

Eleven different sets of propagation conditions were run with the HPM and its component FFP and ray trace models for four different source heights, using a 747-400 aircraft spectrum. The results of the cases were analyzed and compared to provide insight into the effects of the different propagation mechanisms on noise level predictions. In order to advance the concept of "intelligent switching" between the component models and full version of the HPM, focus was placed on identifying conditions that did not require use of the full HPM.

It was found that there are, in fact, opportunities for the use of a single, faster component model, in place of the full HPM. The straight-ray model can be used under simple propagation conditions with a homogeneous atmosphere and finite impedance ground, without range-dependent effects. The FFP model can be used under refractive atmosphere conditions without range-dependent effects. Even further, for higher altitude sources, the impact of range-dependence effects often becomes negligible. In many such cases, the ray model or FFP could be substituted, despite their failure to include range-dependent effects. However, certain points of caution are offered to avoid applying a simpler model where the full model is needed. The major categories for which care should be taken before applying a simpler model include line of sight obstructions between source and receiver, shallow angles of reflection off the ground, and close proximity to ground impedance transitions.

7. FUTURE WORK

In its current state, the HPM is a standalone noise model that accepts AEDT noise source input and utilizes some functional switching between different noise propagation methods depending on source and receiver geometry. Although the HPM could be implemented into AEDT in the near term, it requires significant computational resources and runtime, to compute noise from a single aircraft event. While this report provides a starting point for development of an "intelligent switching" protocol, this protocol has not been fully developed nor implemented in the HPM, and a more thorough investigation into the "switching" criteria should be conducted. The protocol will likely be highly dependent on the relationship between dimensions of source height, propagation range, terrain feature height, distance from ground transitions, etc. The work presented in this report can help direct efforts in the further development of this scheme.

In the near term, runtime concerns may best be addressed by moving toward an advanced ray model, capable of including terrain, ground transitions, and atmospheric effects. In this report, a basic straight-ray model was found to be sufficiently accurate under the simpler propagation conditions. Incorporating the effects of additional propagation mechanism would increase accuracy, while maintaining runtimes that are more manageable than those of the FFP or full HPM. Volpe has access to ray models, Nord2000[10,11], NMSim[12] and AERNOM[13]. These models could be considered for use as a starting point in development of a ray model for integration into the AEDT.

In addition to the effort of developing the intelligent switching concept, other code implementations could be pursued to further reduce runtimes. Such an effort could involve the use of Graphics Processing Units (GPUs). General Programming on the Graphics Processing Unit (GPGPU) consists in developing non-graphical programs on the GPU, to take advantage of the highly parallel processor for computational tasks such as ray tracing or collision detection. The latest GPUs have been designed with such scientific applications in mind, providing double precision computation units. The Compute Unified Device Architecture (CUDA) toolkit (developed by NVIDIA) has now reached significant maturity and is used in a very wide variety of scientific applications. For similar hardware cost, the speedup typically achieved vary from 3 to 20 times faster depending on the degree of parallelism achieved in the algorithm ported to CUDA.

GPGPU is highly applicable to computational atmospheric acoustics. The 2D Parabolic Equation method (PE) requires time proportional to the square of the single frequency considered, and time proportional to the height and the range of the modeled space. Sparse matrix solver libraries available for CUDA or part of the toolkit should enable a very significant improvement in performance. Once these performance improvements are validated, the program may be expanded into supporting multiple nodes for processing of larger cases on a cloud computing platform.

Finally, the testing interface developed to run the HPM with easier integration with the AAM offers an automated way of running the propagation model for the conditions of a real airport. Conducting HPM runs for real-world propagation conditions could provide more insight into the combination of propagation effects (and their magnitude) that one might expect to see under realistic conditions. In the testing interface implementation, users may choose a grid float terrain file, just as they would for the INM. The testing interface combines the terrain file data and

source-receiver geometry data from the “flight.pth” file to generate the appropriate terrain inputs for the HPM. The testing interface implementation, therefore, brings the HPM closer to modeling realistic aviation noise propagation conditions, and also fitting more seamlessly into the AEDT structure.

8. REFERENCES

1. Rosenbaum, J. E., A. A. Atchley, and V. W. Sparrow, "Enhanced sound propagation modeling of aviation noise using a hybrid Parabolic Equation-Fast Field Program method," Inter-Noise conference proceedings, Ottawa, ON (2009).
2. Rosenbaum, J. E., "Enhanced propagation modeling of directional aviation noise: A hybrid parabolic equation-fast field program method," Ph.D. dissertation, The Pennsylvania State University (2011).
3. Rosenbaum, J. E., E. R. Boeker, A. Buer, P. J. Gerbi, C. S. Y. Lee, C. J. Roof, G. G. Fleming, "Assessment of the Hybrid Propagation Model, Volume 2: Comparison with the Integrated Noise Model," Draft Report, Washington, D.C., Federal Aviation Administration (2012).
4. West, M., K. Gilbert, and R. A. Sack, "A tutorial on the parabolic equation (PE) model used for long range sound propagation in the atmosphere," Applied Acoustics, **37**(1), 31-49.
5. Sack, R. A., and M. West, "A parabolic equation for sound propagation in two dimensions over any smooth terrain profile: the generalized terrain parabolic equation (GT-PE)," Applied Acoustics, **45**(2), 113-129 (1995).
6. Salomons, E. M., *Computational Atmospheric Acoustics*, Kluwer Academic Publishers (2001).
7. Franke, S. J. and G. W. Swenson, Jr., "Brief tutorial on the Fast Field Program (FFP) as applied to sound propagation in the air," Applied Acoustics, 27(3), 203-215 (1989).
8. West, M., R. A. Sack, and F. Walkden, "The Fast Field Program (FFP). A second tutorial: Application to long range sound propagation in the atmosphere," Applied Acoustics, 33(3), 199-228 (1991).
9. Attenborough, K., S. Taherzadeh, H. E. Bass, X. Di, R. Raspet, G. R. Becker, A. Güdesen, A. Chrestman, G. A. Daigle, A. L'Espérance, et al., "Benchmark cases for outdoor sound propagation models," J. Acoust. Soc. Am., **97**(1), 173-191 (1995).
10. Plovsing, B. and J. Kragh, "Nord2000. Comprehensive Outdoor Sound Propagation Model. Part 1: Propagation in an Atmosphere without Significant Refraction," DELTA Acoustics & Vibration Report AV 1849/00 (2001).
11. Plovsing, B. and J. Kragh, "Nord2000. Comprehensive Outdoor Sound Propagation Model. Part 2: Propagation in an Atmosphere with Refraction," DELTA Acoustics & Vibration Report AV 1851/00 (2001).
12. Ikelheimer, B. and K. Plotkin, "Noise Model Simulation (NMSim) User's Manual," Wyle Laboratories Report WR 03-09 (2005).
13. Poulain, K., "Numerical propagation of aircraft en-route noise," Masters of Science Thesis, The Pennsylvania State University (2011).